Underwater Localization of Passive Targets Using Spatially Distributed Acoustic Backscatter Tags

Nazish Naeem,[1] Rohan Menon,[1] and Fadel Adib[1,2]

[1] *Electrical Engineering and Computer Science, Massachusetts Institute of Technology, Cambridge, MA 02139, USA*

[2] *Cartesian Systems, Cambridge, MA 02139, USA*

(Dated: 7 November 2026)

Underwater localization of passive targets is important for marine biology, environmental monitoring, coastal resilience, offshore energy, and defense. Conventional approaches rely on active transmissions, but their resolution degrades with distance. To address this limitation, traditional systems use multi-element transmit or receive arrays to improve spatial diversity and localization resolution, at the cost of higher power consumption and expense. This article presents an alternative approach that uses a single acoustic transmitter-receiver pair together with spatially distributed, ultra-low-power underwater backscatter tags to provide greater geometric diversity with marginal impact on power consumption or cost. The tags modulate and reflect incident acoustic waves, generating structured echoes that can be separated and coherently combined to infer target location, effectively emulating a larger active array. We develop an end-to-end theoretical model by extending classical sonar equations to account for the differential scattering cross section of backscatter tags. The model is validated experimentally in a river channel, where predicted and measured responses differ by less than 0.8 dB and 0.2 dB in median across different distances and operating frequencies, respectively. We also demonstrate a proof-of-concept prototype for two-dimensional localization of passive targets. Together, these results highlight the potential of low-cost, low-power localization for long-term underwater monitoring.

I. INTRODUCTION

Localizing passive underwater targets is of great importance to marine biology, aquaculture, environmental monitoring, bathymetry, infrastructure monitoring, and defense. For instance, in aquaculture farms, localization of passive targets can help track fish to study feeding patterns and detect net damage by monitoring unusual movements. In the context of infrastructure maintenance, it can support tasks such as localizing divers during maintenance operations or tracking quiet vessels (e.g., submarines) in sensitive areas. In naval defense, passively localizing underwater vehicles provides significant maritime domain awareness, helping identify vessel locations and adversarial activity.

Underwater acoustic positioning systems, such as LBL[1], SBL[2], and USBL[3], are commonly used to track underwater vehicles and divers. However, these systems require the target to be equipped with a transponder and therefore cannot localize passive targets. The dominant approach for localizing passive targets today relies on active SONAR[4]: a transmitter emits pulses and a receiver, often a hydrophone array, measures the returned echoes to estimate time of flight and angle of arrival, shown in Fig. 1a. This approach encompasses a broad category of methods including hydrophone arrays[5], vector hydrophones[6,7], and silent SONAR[8]. The resolution of these methods, however, deteriorates with distance to the target[9].

To overcome this resolution deterioration, another approach involves deploying multiple SONAR systems to cover different areas of interest and/or adopting multistatic deployments that involve multiple spatially separated transmit and receive nodes to maintain illumination and geometric diversity[10], as shown in Fig. 1b. Because of the potential of multistatic ap-

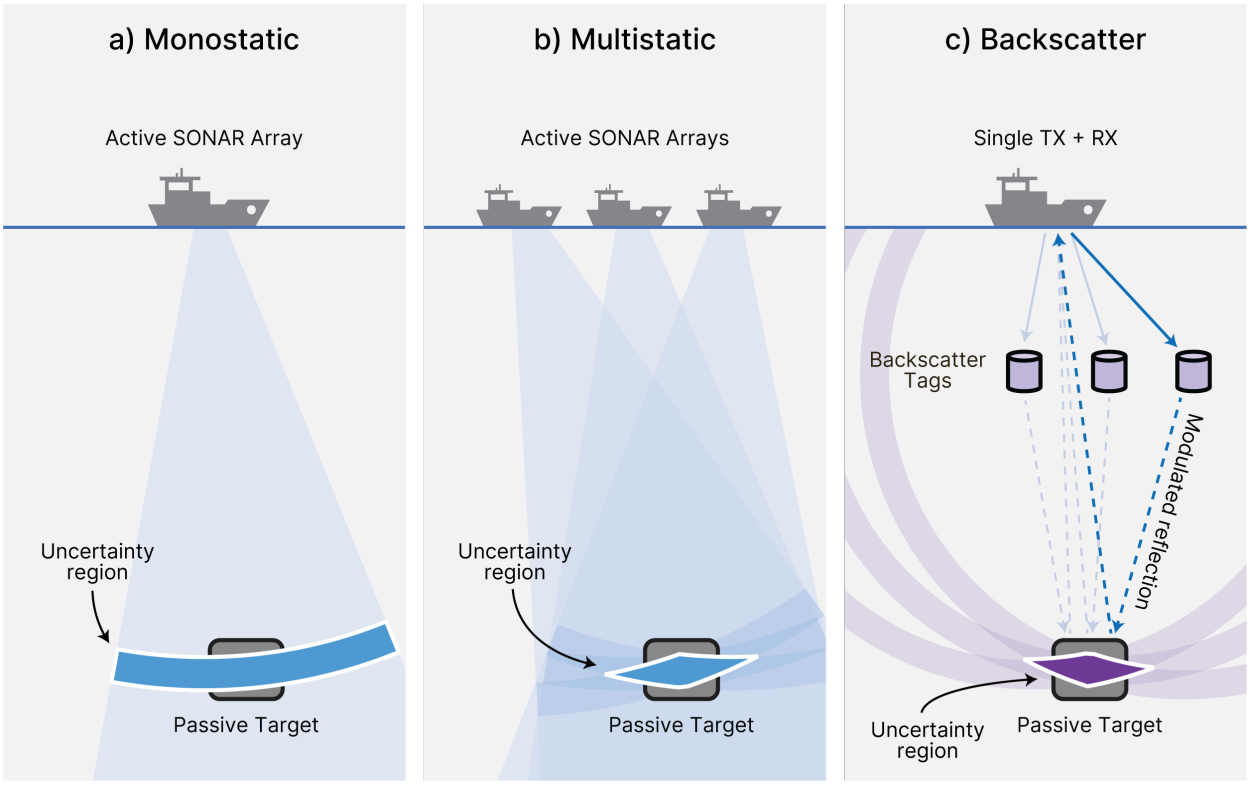

FIG. 1. **Passive target localization architectures.** **(a)** A monostatic sonar localizes a passive target from its direct echo, with resolution degrading at longer ranges. **(b)** A multistatic deployment improves geometric diversity using multiple active sonar nodes, at the cost of higher power and hardware complexity. **(c)** The proposed architecture uses one active transceiver and multiple passive backscatter tags. Combining backscatter range estimates enables localization.

proaches, substantial prior work has focused on improving localization algorithms, including weighted least squares[11,12], Bayesian methods[13], multi-hypothesis tracking (MHT)[14], sensitivity kernels[15], and machine learning based approaches[16]. However, the infrastructure cost of creating this diversity remains largely unaddressed: each additional node increases system cost, power consumption, and deployment/logistics complexity.

In this article, we ask the following question: Is it possible to increase localization resolution without significantly increasing power, cost, and logistical burden? A positive answer would suggest that high-resolution localization can be made more practical in power- and cost-constrained ocean environments. To this end, this article presents an alternative passive target localization approach that replaces conventional multistatic deployments with a network of spatially distributed, independently deployed passive acoustic backscatter tags placed throughout the environment, while requiring only a single transceiver, as shown in Fig. 1c. Backscatter is a recent communication technique in which a tag modulates and reflects existing acoustic transmissions, rather than generating them, enabling orders-of-magnitude lower power consumption than traditional acoustic modems[17]. Moreover, because a backscatter tag consists primarily of a piezoelectric transducer and simple low-power switching circuitry, it can also be realized at low cost. Its ultra-low-power, low-cost operation not only makes it practical to add spatial diversity with minimal cost and power overhead, but also allows the deployment of these backscatter tags closer to the target for improved resolution.

The core idea of the proposed method is to increase the number of vantage points in the environment via backscatter tags, to localize a passive target. To understand the proposed method, consider a single backscatter tag in the environment. As shown in Fig. 3, when the transmitter emits an acoustic signal, it propagates through the environment. Some of the signal, as shown in Fig. 3a, travels toward the target object and reflects back to the receiver. This received echo encodes the target's round trip distance from the transceiver through its time of flight. In the presence of a backscatter tag, another portion of the

transmitted signal, as shown in Fig. 3b, reaches the tag and is reflected in the environment. For a typical backscatter tag, a portion of this reflection returns directly to the transceiver, while most of it continues to propagate into the environment, reflects off surrounding objects, and then reaches the receiver. This creates additional propagation paths, which are typically undesirable for communication and are therefore suppressed in prior work[18,19]. In the proposed method, we exploit these secondary reflections because the time of flight of these tag-mediated reflections encodes the target's distance relative to the tag. As a result, even a single backscatter tag provides additional geometric diversity beyond the direct echo, enabling 2D localization of the target. The proposed method extends this core idea to multiple independently modulated backscatter tags, which generate tag-specific echoes that are separable at the receiver. Once separated, these echoes can be processed and combined to form a larger virtual aperture, yielding improved geometric diversity and higher localization resolution. Section III details the proposed localization method.

To evaluate the fundamental bounds of the proposed method, this work develops a closed form end-to-end theoretical model of underwater backscatter-tag-based passive target localization. This allows us to determine how the performance of such a system depends on various system characteristics like the differential scattering cross-section of the backscatter tag, propagation channel, operating frequency, target strength of the reflectors, and other system parameters. Prior work[20,21] has developed link-budget models for underwater backscatter nodes but these models focus on communication rather than localization. As a result, they consider only the direct communication path and largely ignore multipath, that is, indirect reflections from targets, which is the central phenomenon exploited by our

proposed passive localization method. Classical SONAR equations, on the other hand, are also insufficient because they do not account for the electro-acoustic modulation introduced by backscatter tags, which is fundamental to our approach.

To bridge this gap between localization and communication, we reformulate SONAR equations to incorporate the backscatter tags' differential scattering cross-section with higher-order reflections, and combine across a distributed aperture. Specifically, we derive a closed-form analytical model that traces the acoustic propagation path of the transmitted signal in the environment in the presence of underwater backscatter tags as secondary transmitters. To do so, we isolate the received signal component that interacts with the tag and model it by tracing the acoustic power flow through the full path, explicitly incorporating the tag's electro-acoustic transduction and the target object's target strength to compute the received signal level, which we call backscatter echo level. We then use this backscatter echo level to derive the signal excess of the system, which defines the performance limits of the proposed method.

We built a prototype of our system and verified our analytical framework for backscatter-based passive target localization model through experimental validation. Our results show that the analytical model matches the experimental results with a median error of 0.8 dB, 0.2 dB and 0.4 dB across different distances, operating frequencies and transmitter source levels. Finally, we demonstrate initial 2D localization results with a median localization error of 7.4 cm.

The rest of the article is organized as follows. §II provides a primer on underwater backscatter tags. §III explains the localization method in the presence of a single backscatter

tag and then extends it to a network of backscatter tags. We then derive the closed-form analytical model of the proposed localization method in §IV. §V describes the experimental setup. §VI, §VII, and §VIII present the experimental validation, localization results, and design tradeoffs of the proposed system. Finally, §IX describes some of the extensions of the proposed method in various configurations.

II. PRIMER ON UNDERWATER BACKSCATTER

Underwater backscatter[17,22] is an emerging technology for ultra-low-power underwater acoustic communication and sensing. Instead of generating its own acoustic signal, a backscatter tag communicates by reflecting existing sound signals. Fig. 2 illustrates this basic operating principle. A typical backscatter tag consists of a piezoelectric transducer, an energy-harvesting circuit, and a switching network. When an incoming acoustic wave impinges on the transducer, the mechanical vibration is converted into an electrical signal. The tag then alternates its electrical load between different impedance states, typically reflective and absorptive, which changes the amount of acoustic energy reradiated back into the environment. By toggling between these states, the tag modulates the reflected wave without generating a carrier of its own, a process known as backscatter. In the absorptive state, part of the incident energy can also be harvested to power the tag's low-power electronics, making sustained operation possible with little to no onboard energy source.

This operating model is fundamentally different from conventional active underwater modems, which must spend significant power to synthesize and transmit acoustic signals. By offloading carrier generation to an external transmitter, underwater backscatter enables net-

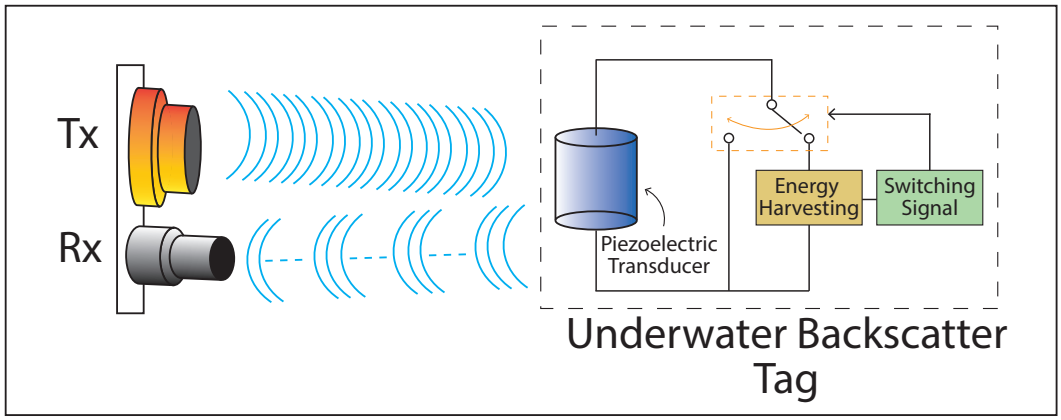

FIG. 2. **Underwater Backscatter Overview.** The backscatter tag consists of a piezoelectric transducer, an energy-harvesting circuit, and a switching circuit. When the transmitter transmits a signal, it reaches the backscatter tag where the backscatter tag harvests energy. This harvested energy is then used to drive the switching circuit. This switching operation modulates the received signal and reflects (backscatters) it back to the receiver.

zero-power operation at the tag, making it attractive for long-term deployments in resource-constrained marine environments. Prior work has shown that such systems can support persistent underwater sensing applications, including environmental monitoring and low-power imaging[18,23–25]. In this article, we leverage the same principle not primarily for data communication, but to create a controllable secondary reflector for localization, as we explain in the following section.

III. TARGET LOCALIZATION WITH A SINGLE BACKSCATTER TAG

To understand how backscatter tags can enable passive target localization, we first describe how traditional systems achieve this. Traditional systems work by emitting an acoustic

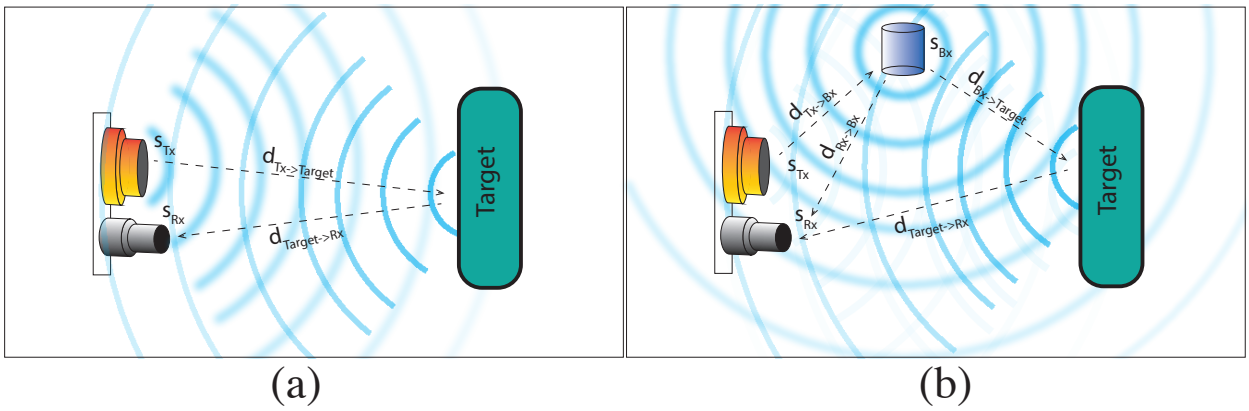

FIG. 3. **Simplified System Overview.** **(a)** Echo sounding in the presence of a single target object. **(b)** Proposed localization method in the presence of a single backscatter tag.

signal (typically a ping) and listening for the echo reflected from a target[26]. The time difference between the transmitted and received signal can be used to determine the round-trip time-of-flight of the signal (i.e., the time it takes the signal to propagate from the transmitter to the target and back to the receiver). This is shown in Fig. 3(a), where the source transmits signal s_{Tx}, which propagates through the environment and gets reflected by the target before it reaches the receiver after time Δt. This round-trip time-of-flight Δt can be used to estimate the target range, as shown below,

$$d_{Tx \to Target \to Rx} = c\Delta t \tag{1}$$

where c is the speed of sound in water and $d_{Tx \to Target \to Rx}$ is the round-trip distance between the transceiver and the target, which equals the sum of $d_{Tx \to Target}$ and $d_{Target \to Rx}$ shown in Fig. 3(a).

When a single backscatter tag is added to the environment, this transmitted acoustic signal also propagates and reaches the tag. When this signal reaches the backscatter tag, it

gets backscattered in all directions, effectively acting as a secondary source that illuminates the environment from a different vantage point. As shown in Fig. 3(b), this backscattered signal propagates isotropically. As a result, part of the signal is received directly by the receiver, while some of the signal propagates through the environment and is reflected by the target back to the receiver. This additional echo from the backscattered signal has a time of flight corresponding to propagation from the source to the backscatter tag, then to the target, and finally back to the receiver. Now, this additional time-of-flight from the backscatter signal, along with the time-of-flight of the direct signal, can be used to determine the 2D location of the target object.

In order to translate this idea into a localization method, a key requirement is that the receiver must be able to not only distinguish different propagation paths, but also determine which of those paths involve the backscatter tag. To do so, the excitation signal and its interaction with the backscatter tag should allow the receiver to isolate and identify the relevant echoes. In the rest of this section, we first describe the choice of excitation signal for the backscatter tag. We then explain how this signal can be used to estimate the distance of an object from a single transceiver. Finally, we describe how a single backscatter node interacts with this excitation signal to determine the range of the target from a different vantage point, enabling localization.

A. Selecting Excitation Signal

The majority of traditional localization methods rely on short pulses (i.e., time-gated pings)[26]. These time-gated transmissions allow the receiver to distinguish different echoes,

with a range resolution that improves as the pulse width decreases. However, such pulses are not well suited to backscatter tags. Recall that a backscatter tag works by reflecting an existing acoustic signal; if the excitation is a short-lived pulse, the tag-assisted return suffers a large SNR penalty, often making the backscatter signal undetectable. In contrast, backscatter systems typically use single-tone continuous waves for communication. While the continuous excitation helps sustain sufficient SNR at the tag, it makes time-of-flight estimation difficult because echoes from different propagation paths overlap in time and therefore do not remain separable. To overcome these challenges, we instead use Frequency-Modulated Continuous-Wave (FMCW) chirps as the excitation signal. FMCW is widely used in radar[27], as well as in active[28–31] and silent SONAR[8]. FMCW signals are continuous in time, while their instantaneous frequency sweeps over a specified bandwidth. Their continuous nature makes them compatible with backscatter tags, while the frequency sweep enables the separation of time-delayed returns even when they overlap in time.

B. FMCW-Based Ranging

Now that we have described the choice of excitation signal, in this section we explain how this excitation signal can be used for target ranging. Consider a situation such as shown in Fig. 3a, where there is a transmitter transmitting an FMCW signal s_{Tx} and a target object in the environment, at a distance $d_{Tx \to Target}$ from the transmitter, that reflects the signal towards the receiver where the receiver receives the signal s_{Rx} after time Δt. The transmitted FMCW signal s_{Tx} can be written as follows:

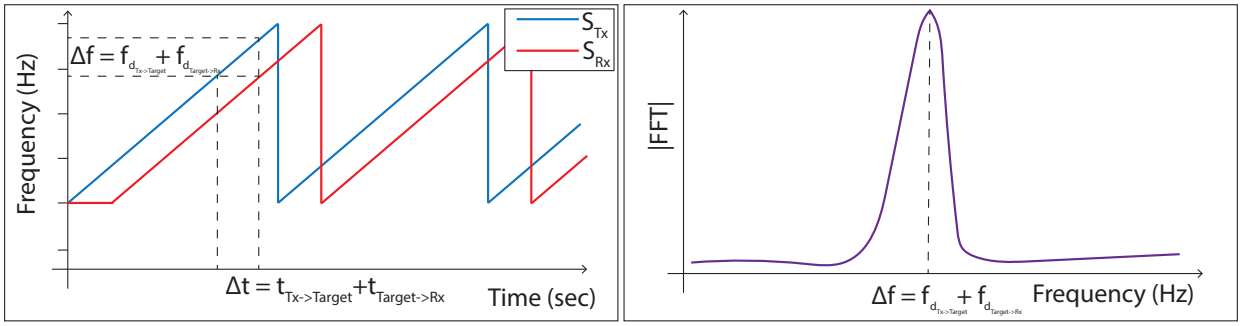

FIG. 4. **FMCW Signal.** Panels (a) and (b) show, respectively, the frequency-versus-time plot of the transmitted FMCW signal (chirp) (s_{Tx}) and received signal (s_{Rx}) from a single reflector, and the frequency response of the received signal after dechirping.

$$s_{Tx}(t) = Ae^{j2\pi(f_c + B\frac{t}{2T})t} \tag{2}$$

where f_c is the start frequency, B is the bandwidth and T is the duration of the transmit signal. Fig. 4a shows the time-frequency plot of the transmitted FMCW signal (blue curve). Since the instantaneous frequency of an FMCW chirp varies over time, it can resolve propagation delays in the received echo even when the echo overlaps in time with the transmit signal. This is illustrated in Fig. 4a, where the red curve shows a time-delayed version of the transmit signal. As seen in the figure, a time delay shifts the chirp to the right on the time axis (i.e., x-axis), therefore, at any given time instant, the delayed and undelayed signals occupy different frequencies, making the two signals separable in the frequency domain.

On a higher level, an FMCW signal transforms a time delay Δt into a frequency shift of Δf. This frequency shift can be found by multiplying the received signal by the complex conjugate of the transmitted signal. This process is called dechirping, which is a type

of pulse compression that enables high resolution ranging while maintaining a high average transmit power compared to a pulse. Mathematically, for a received signal $s_{Rx}(t) = A'e^{j2\pi(f_c+B\frac{(t-\Delta t)}{2T})(t-\Delta t)}$, the dechirped signal is written as,

$$\begin{aligned} s_{dechirped} &= s_{Rx}(t) \times s^*_{Tx}(t) \\ &= A'e^{j2\pi(f_c+B\frac{(t-\Delta t)}{2T})(t-\Delta t)} \times Ae^{-j2\pi(f_c+B\frac{t}{2T})t} \\ &= AA'e^{\Phi} \times e^{j2\pi\Delta ft} \end{aligned}$$

where $\Phi = j2\pi(\frac{B\Delta t}{2T} - f_c)\Delta t$ and $\Delta f = B\frac{\Delta t}{T}$ are the phase and frequency of the dechirped signal. From Eqn. 1, Δf can be written as;

$$\Delta f = B\frac{d_{Tx\to Target\to Rx}}{T \times c} \tag{3}$$

For a collocated transmitter and receiver, or transceiver, $d_{Tx\to Target} \approx d_{Target\to Rx}$, and therefore the above equation becomes,

$$\Delta f = 2B\frac{d_{Tx\to Target}}{T \times c} \tag{4}$$

This frequency shift can be found by computing the magnitude of the Fourier transform of the dechirped signal as shown in Fig. 4b. Essentially, this dechirped signal gives the impulse response of the environment with frequency peaks corresponding to the distances of the reflectors from the transceiver.

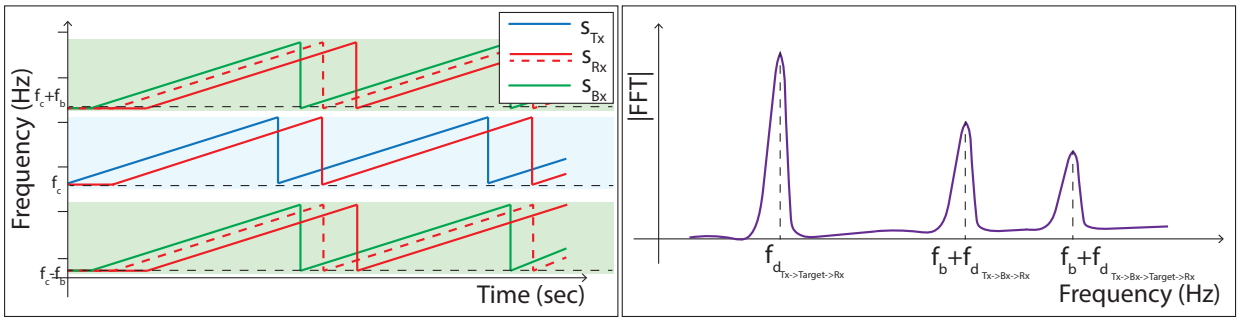

FIG. 5. **FMCW Signal with Backscatter Modulation.** a) shows the frequency vs time plot of the transmitted FMCW signal (chirp) (s_{Tx}), backscattered (s_{Bx}) and received (s_{Rx}) signal in the presence of a single backscatter tag and a single reflector in the environment and b) shows the frequency response of the received signal after dechirping.

C. Backscatter Tag as Secondary FMCW Source

Now that we have described how FMCW-based ranging works, in this section we explain how a single backscatter tag in the environment interacts with the FMCW excitation signal to provide geometric diversity for target localization.

As shown in Fig. 3b, when a backscatter tag is present, the transmitted signal is reflected not only by the target but also by the tag, which backscatters the transmitted signal modulated by the tag's switching signal. The tag does so by switching its acoustic load between two states (reflective and absorptive) using a square-wave control signal at a specified switching frequency, f_b. This switching mixes the incident FMCW signal with a periodic waveform and produces frequency-shifted replicas of the FMCW signal. Specifically, the tag shifts the original start frequency f_c of the transmitted signal to $f_c + f_b$ and $f_c - f_b$. Fig. 5a

shows the frequency-time plot of the transmitted chirp (blue solid curve) and the backscattered signal (green solid curve). Note that the backscattered signal is not only shifted (up and down) in frequency by f_b but is also delayed in time corresponding to the time it takes the transmit signal to reach the backscatter tag. Mathematically, for a backscatter tag at a distance of $d_{Tx\to Bx}$ from the transmitter (as shown in Fig. 3b) with a corresponding time delay of $t_{Tx\to Bx}$, the backscattered signal s_{Bx} can be written as:

$$s_{Bx}(t) = s_{Tx}(t - t_{Tx\to Bx}) \times m(t) \tag{5}$$

where $m(t)$ is the modulation signal given by: $m(t) = \frac{4}{\pi}\sum_{l=1,3,5...}^{\infty}\frac{1}{l}\sin(2\pi l f_b t)$ where higher-order terms $l > 3$ can be ignored due to decreased strengths[20] and s_{Bx} becomes,

$$\begin{aligned} s_{Bx}(t) &= \alpha s_{Tx}(t - t_{Tx\to Bx})\sin(2\pi f_b t) \\ &= \alpha(s_{Tx}(t - t_{Tx\to Bx}) * e^{j2\pi f_b t} \\ &+ s_{Tx}(t - t_{Tx\to Bx})) * e^{-j2\pi f_b t}) \end{aligned} \tag{6}$$

where α is the amplitude of the signal. The above equation shows that the backscattered signal s_{Bx} is a time-delayed chirp upshifted by f_b. By choosing $f_b > B$, we can ensure the spectral separability between the transmitted FMCW signal and the backscattered FMCW signal.

Now this signal s_{Bx}, which acts as a secondary FMCW signal, propagates in the environment similar to the transmitted signal s_{Tx}. As shown in Fig. 3b, part of this signal travels back to the receiver, while most of it propagates through the environment, where a portion is reflected by the target. These two received signals are shown in Fig. 5a as red dotted and red solid curves, respectively, in the green highlighted areas of the plot as time delayed

versions of s_{Bx}. Recall that the transceiver's signal propagation also results in an echo of the transmitted signal, caused by the target, to be received at the receiver. This signal, the direct path, is shown as a red solid curve in the blue highlighted area in Fig. 5a. The receiver receives the sum of all these received signals (red solid and dotted curves in Fig. 5a) which is then dechirped to estimate the frequency delays to determine the target location. The frequency transform of this dechirped signal is shown in Fig. 5b. When dechirped with the complex conjugate of the transmitted signal, this produces three frequency peaks[32] corresponding to the three signal paths. These frequencies together are then used to estimate the target location.

Along with enabling ultra-low-power operation, the use of backscatter tags provides two additional benefits. First, since the tags reflect the original transmitted signal, the resulting echoes remain coherent with the source, reducing the challenges associated with frequency synchronization and locking while also preserving SNR benefits from precise frequency alignment. Second, backscatter tags can be implemented using simple hardware, since they do not need to independently generate or amplify acoustic signals, making them easier to build and deploy. Moreover, array-based backscatter structures[19] can provide a gain greater than 0 dB without requiring active amplification, enabling higher SNR responses.

D. Localization from Two Vantage Points

We can use the frequencies estimated in the previous section to estimate the location of the target from two vantage points. Specifically, we can use the frequency-distance relation from Eqn. 3 to estimate the distances $d_{Tx\rightarrow Target\rightarrow Rx}$ and $d_{Tx\rightarrow Bx\rightarrow Target\rightarrow Rx}$ as follows:

$$d_{Tx\to Target\to Rx} = \frac{f_{d_{Tx\to Target\to Rx}} \times T \times c}{B}$$

$$d_{Tx\to Bx\to Target\to Rx} = \frac{f_{d_{Tx\to Bx\to Target\to Rx}} \times T \times c}{B}$$

For a collocated Tx and Rx, the distance between the transceiver (TRx) and target can be estimated as $d_{Tx\to Target} = \frac{d_{Tx\to Target\to Rx}}{2}$. With this distance estimate, the target can lie anywhere on a circle (in 2D) with radius $d_{Tx\to Target}$ and center at TRx. With a second distance estimate, $d_{Tx\to Bx\to Target\to Rx}$, we can use the known location of the TRx and backscatter to calculate $d_{Bx\to Target\to Rx}$ (the sum of the distances $d_{Bx\to Target}$ and $d_{Target\to Rx}$). With this distance estimate, in 2D, we can construct an ellipse with the backscatter tag and TRx at the foci of the ellipse and $d_{Bx\to Target\to Rx}$ being the sum of focal radii ($d_{Bx\to Target}$ and $d_{Target\to Rx}$) with the target lying on the ellipse. We can use this information to construct a probability map of the target location in the 2D plane. Fig. 6a shows a similar 2D probability map created in simulation for a single backscatter tag (blue dot) submerged in the environment with a transceiver (black dot) and a target object (white cross). The figure shows that the presence of a single backscatter tag in the environment improves the 2D location estimate from a circle to two candidate points (shown as dotted red circles). Fig. 6b shows that with the addition of another backscatter tag, the location estimate can be further improved to a single point.

Network of Backscatter Tags. Building on the simple setup, as shown in Fig. 6, we can use a network of backscatter tags to improve both coverage and localization accuracy in three dimensions. Specifically, each backscatter tag with its unique switching rate can be employed to produce separable secondary transmissions, yielding additional vantage points

ALGORITHM 1: Distance estimation from the received signal

Require: Received signal $s_{Rx}(t)$, transmitted FMCW signal $s_{Tx}(t)$, chirp bandwidth B, chirp duration T, speed of sound c, transceiver location $\mathbf{p}_{TRx}$, backscatter tag locations $\{\mathbf{p}_{Bx,i}\}_{i=1}^{N}$, and switching frequencies $\{f_{b,i}\}_{i=1}^{N}$.

Dechirp the received signal:

$$s_{\text{dechirped}}(t) = s_{Rx}(t)s_{Tx}^{*}(t).$$

Compute the magnitude spectrum:

$$S(f) = \left|\mathcal{F}\{s_{\text{dechirped}}(t)\}\right|.$$

Direct target-path distance:

Search $S(f)$ near $f = 0$ and identify the target-reflection peak $f_{d_{Tx\to Target\to Rx}}$.

Convert the peak frequency to the direct path length:

$$d_{Tx\to Target\to Rx} = \frac{f_{d_{Tx\to Target\to Rx}} \times T \times c}{B}.$$

For a collocated transmitter and receiver, compute:

$$d_{Tx\to Target} = \frac{d_{Tx\to Target\to Rx}}{2}.$$

Backscatter-assisted target-path distances:

for $i = 1, \ldots, N$ **do**

Search $S(f)$ in the neighborhood of the switching frequency $f_{b,i}$.

Identify the peaks corresponding to the known $Tx \to Bx_i \to Rx$ path and unknown $Tx \to Bx_i \to Target \to Rx$ path.

Remove the switching-frequency offset:

$$\Delta f_i = \left|f_{Target,i} - f_{b,i}\right|.$$

Convert the frequency shift to propagation path length:

$$d_{Tx\to Bx_i\to Target\to Rx} = \frac{\Delta f_i T c}{B}.$$

Compute the known Tx-to-tag distance:

$$d_{Tx\to Bx_i} = \left\|\mathbf{p}_{TRx} - \mathbf{p}_{Bx,i}\right\|.$$

Remove the known Tx-to-tag distance:

$$d_{Bx_i\to Target\to Rx} = d_{Tx\to Bx_i\to Target\to Rx} - d_{Tx\to Bx_i}.$$

end for

Result: $d_{Tx\to Target}$ and $\{d_{Bx_i\to Target\to Rx}\}_{i=1}^{N}$.

for improved performance. The distance estimation and consequent localization algorithms for a network of backscatter tags are presented in detail in Algorithm 1 and Algorithm 2 respectively.

Having outlined the principle of the proposed localization method, we now examine its feasibility and fundamental limits. In the following section, we address these questions by deriving the analytical model for the proposed target localization method.

ALGORITHM 2: Target localization from estimated distances

Require: Direct target distance $d_{TRx\to Target}$, backscatter-assisted distances $\{d_{Bx_i\to Target\to Rx}\}_{i=1}^{N}$, transceiver location $\mathbf{p}_{Tx}$, and backscatter tag locations $\{\mathbf{p}_{Bx,i}\}_{i=1}^{N}$.

1: Construct a circular constraint probability map centered at $\mathbf{p}_{TRx}$ with radius $d_{TRx\to Target}$.

$$P(\mathbf{p}) = e^{\frac{-(d_{TRx\to Target}-d(\mathbf{p}))^2}{2\sigma^2}}$$

where $d(\mathbf{p}) = \|\mathbf{p}_{TRx} - \mathbf{p}\|$ and σ is the standard deviation

2: **for** $i = 1, \ldots, N$ **do**

3: Construct an elliptical constraint probability map with foci at $\mathbf{p}_{Bx,i}$ and $\mathbf{p}_{TRx}$.

$$P_e(\mathbf{p}) = e^{\frac{-(d_{Bx_i\to Target\to Rx}-d(\mathbf{p}))^2}{2\sigma^2}}$$

where $d(\mathbf{p}) = \|\mathbf{p}_{TRx} - \mathbf{p}\| + \|\mathbf{p}_{Bx,i} - \mathbf{p}\|$

4: Combine the probabilities

$$P(\mathbf{p}) = P(\mathbf{p}) \times P_e(\mathbf{p})$$

5: **end for**

6: Estimate the target location as:

$$\hat{\mathbf{p}}_{Target} = \arg\max_{\mathbf{p}} P(\mathbf{p}).$$

Return: $\hat{\mathbf{p}}_{Target}$.

IV. ANALYTICAL MODEL

Analytical modeling is crucial for characterizing underwater acoustic localization systems because it relates system parameters, such as transmitted acoustic signal power, propagation loss, and noise, to performance metrics including detection range and signal-to-noise ratio (SNR). In this section, we analyze the power flow of the acoustic signal propagation in the proposed method to derive a closed-form analytical model.

Recall from the previous section that the presence of a backscatter tag in the environment modulates and redirects the transmit signal from a new vantage point. Therefore, to derive the analytical model, we must trace the power flow that captures these vantage points. The

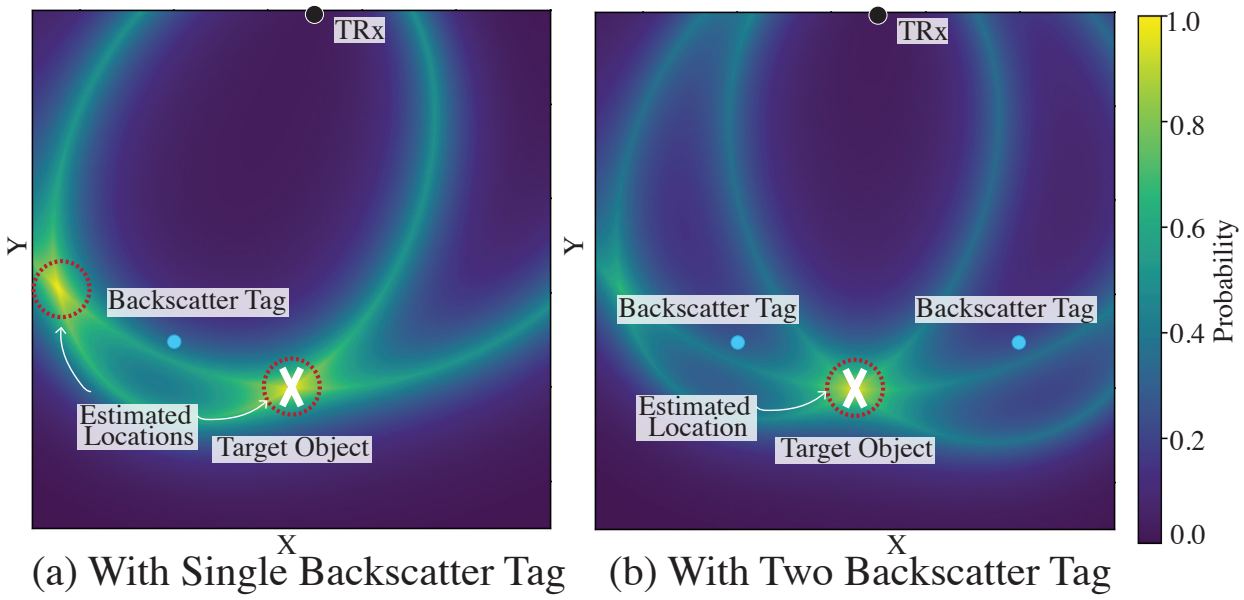

FIG. 6. **Localization Heatmaps. (a)** in the presence of a single backscatter tag in the environment and **(b)** in the presence of two backscatter tags in the environment.

first step in modeling is to determine the received signal levels from the reflections. This received signal level is called echo level (EL) which is defined as the intensity of the received acoustic signal that is returned after reflecting off a target, measured in dB. In a traditional localization system (with a single active transceiver) as shown in Fig. 7a, EL is given by[33]:

$$EL = SL - 2PL(d_{Tx \to Target}, f) + TS \tag{7}$$

Where SL is the source level, $PL(d_{Tx \to Target}, f)$ is the one-way path loss and TS is the target strength of the object. This equation follows directly from tracing the signal power along the traveled distance. Specifically, as shown in Fig. 7a, the transmitter transmits an acoustic signal which is characterized by source level (SL). SL is defined as the far-field pressure level generated by the transducer, measured at 1 m from the transducer[33], in $dB\ re\ 1\mu Pa$. It is a function of input electrical power (P_{elec}) in watts, electromechanical

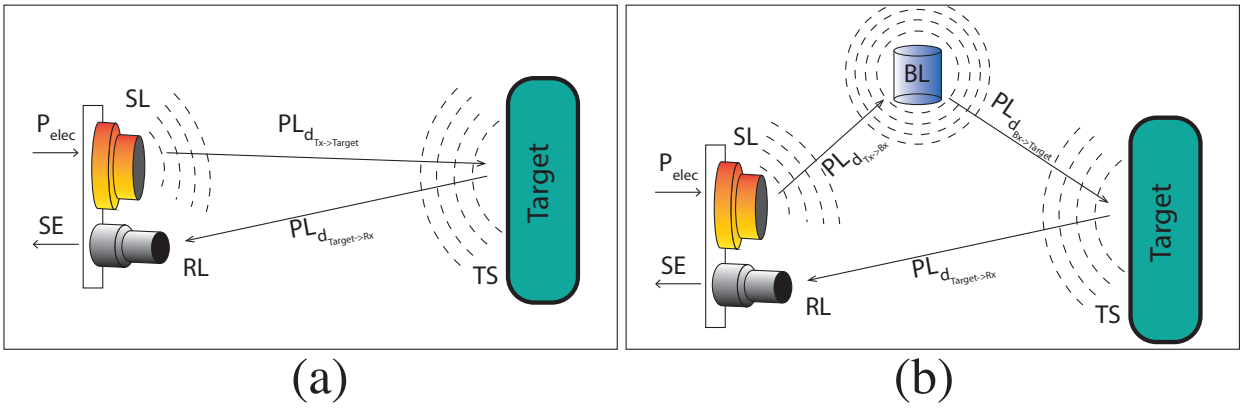

FIG. 7. **Power Flow. (a)** shows the power flow during the signal propagation in the presence of a target object in the environment. **(b)** shows the power flow in the presence of a single backscatter tag and a target in the environment.

efficiency of the transducer (η_{Tx}), and the transducer's directivity index (DI) measured in dB. Mathematically, it is given by[33]:

$$SL = 170.8 + 10\log(\eta_{Tx} P_{elec}) + DI \tag{8}$$

where 170.8 is the conversion constant used to express acoustic source level in $dB\ re\ 1\mu Pa$ from electrical transmit power in watts[33]. Now, as the wave propagates from the transducer to the target at a distance $d_{Tx \to Target}$, it attenuates by a one-way path loss $PL(d_{Tx \to Target}, f)$. Mathematically, PL is given as[33],

$$PL(d_{Tx \to Target}, f) = k \times 10\log(d_{Tx \to Target}) + \alpha(f) d_{Tx \to Target} \tag{9}$$

Where k is the spreading factor, f is the operational frequency, $\alpha(f)$ is the frequency-dependent absorption coefficient. When the signal reaches the target, it reflects a fraction

of the incident energy, characterized by the target strength (TS), which is defined as the *log* of the ratio of the reflected intensity, measured at 1 m from the acoustic center of the target, to the incident intensity. Mathematically defined as follows[33]:

$$TS = 10\log(\frac{I_r}{I_i}) \tag{10}$$

Where I_i and I_r are the incident and reflected intensity of the acoustic signal respectively. TS encapsulates the physical properties of the target object and depends on its shape, size, material properties, and the incident signal angles.

Finally, the reflected wave experiences the same propagation loss (for a collocated Tx and Rx) on the return path to the receiver, contributing a second $PL(d_{Tx\rightarrow Target}, f)$. Combining these steps yields the EL as described in Eqn. 7.

A. Backscattered Echo Level

So far, we have described how the EL is defined for traditional localization systems. In this section, we re-derive EL for the proposed localization method i.e., in the presence of a backscatter tag. To do so, we isolate the component of the received signal that is responsible for providing the backscatter-aided range estimate. This signal path is also shown in Fig. 7b, where the transmitter transmits a signal, which propagates towards the backscatter tag, and gets modulated to re-radiate a secondary chirp (as described by Eqn. 6) isotropically before reaching the target. In order to compute the EL associated with this signal path, we first find the effective source level of the signal reaching the target. This effective source level

can be computed using backscatter level (BL). BL is defined as the acoustic pressure level at the receiver due to the backscatter signal. Formally[20]:

$$BL = 159.8 + 10\log(\eta_{Tx} P_{elec}) + DI_{Tx} + 10\log(\sigma) + DI_{Bx} \\ -2PL(d_{Tx\to Bx}, f) \tag{11}$$

Where P_{elec} and η_{Tx} are the input electrical power and efficiency of the transmitter respectively. DI_{Tx} and DI_{Bx} are the directivity index of the transmitter and backscatter tag respectively. $PL(d_{Tx\to Bx}, f)$ is the one way path loss experienced by the acoustic signal and σ is the backscattering cross section of the backscatter tag, which incorporates the electromechanical coupling of the backscatter tag. The constant 159.8 is derived from the conversion constant in Eqn. 8 when computing the corresponding backscatter level[20]. This expression can be further simplified to,

$$BL = 159.8 + 10\log(P_{elec}) + G_{Tx} + 10\log(\frac{\lambda^2}{\pi}) + 2G_{Bx} \\ -2PL(d_{Tx\to Bx}, f) + IML_u \tag{12}$$

where λ is the wavelength of the operational frequency, G_{Tx} and G_{Bx} are the gains of the transmitter and backscatter tag respectively, and IML_u represents the logarithmic loss due to impedance mismatch which can be calculated by measuring the electrical impedance of the backscatter transducer and the switched electrical load separately.

Importantly, this expression for BL provides the received level of the backscattered signal that arrives at the receiver under the simplified assumption that the tag is equidistant from the transmitter and the receiver. Under this assumption, the backscattered signal experiences a round-trip propagation loss of $2PL(d_{Tx\to Bx}, f)$. However, to use this quantity

in the EL formulation, we require an equivalent effective source level referenced at $1m$ from the source. Accordingly, BL can be rewritten as:

$$BL = 159.8 + 10\log(P_{elec}) + G_{Tx} + 10\log(\frac{\lambda^2}{\pi}) + 2G_{Bx} \\ -PL(d_{Tx\rightarrow Bx}, f) + IML_u \tag{13}$$

Using Eqn. 7 the EL equation becomes,

$$EL = 159.8 + 10\log(P_{elec}) + G_{Tx} + 10\log(\frac{\lambda^2}{\pi}) + 2G_{Bx} \\ -2PL(d_{Tx\rightarrow Bx}, f) + IML_u - PL(d_{Bx\rightarrow Target}, f) \\ -PL(d_{Target\rightarrow Rx}, f) + TS \tag{14}$$

Where $PL(d_{Bx\rightarrow Target}, f)$ and $PL(d_{Target\rightarrow Rx}, f)$ are the path loss corresponding to the distance $d_{Bx\rightarrow Target}$ and $d_{Target\rightarrow Rx}$ traversed by the acoustic signal from backscatter tag to the target and target to the receiver respectively. The equation above defines the backscatter echo level in terms of the known electro-acoustic properties of the transducers (e.g., the transmitter input power, transducer gains, and impedance mismatch loss). These properties are easy to quantify both experimentally and numerically [20].

B. Backscatter Signal Excess (SE)

Now that we have determined the backscatter EL, we use it to determine the signal excess (SE) of the system. Traditional localization systems express the difference between the signal-to-noise ratio (SNR) of the received signal at the receiver and the detection threshold (DT) as SE of the system in dB. Mathematically expressed as,

$$\begin{aligned} SE &= SNR - DT \\ &= EL - N - DT \end{aligned} \tag{15}$$

Here, N denotes the noise level in the frequency band of interest. It includes both ambient acoustic noise in the environment and electrical noise at the receiver. Depending on the system setup, operating environment (ocean, river, or lake), and nearby noise sources such as shipping or boating activity (and their type and proximity), N can be determined experimentally.

Impact of Self-Interference Noise: The preceding analysis assumes that the received backscatter signal is limited only by the ambient and receiver noise captured by N. However, since the transmitter and receiver are collocated, the direct signal path between the Tx and Rx results in self-interference (SI) noise. This additional interference reduces the effective signal-to-interference-plus-noise ratio (SINR) available for detecting the backscatter signal. Accordingly, in the presence of self-interference, the signal excess can be expressed as

$$SE = EL - N - SINL - DT \tag{16}$$

where SINL, the self-interference noise level, is defined as[21]

$$SINL = 170.8 + 10\log(P_{elec}) + G_{Tx_{90}}(P_{elec}) + PL_n \tag{17}$$

Where PL_n denotes the path loss experienced by the direct path and $G_{Tx_{90}}(P_{elec})$ is the gain of the transmitter in the direction of the receiver. Note that $G_{Tx_{90}}(P_{elec})$ is a function of the input electrical power and depends on factors such as the amplifier noise, phase noise and cavitation[21]. This self-interference, when within the dynamic range of the receiver, can be

easily mitigated digitally via techniques like background subtraction, filtering, or coherent cancellation using the known transmitted waveform. However, sufficiently high source levels may saturate the receiver front-end, in which case state-of-the-art underwater backscatter communication[19] uses physical isolation to minimize the interference. Note that Eqn. 16 is only applicable if $SINL$ is comparable to or greater than N. In the case where $SINL < N$, SE is defined by Eqn. 15.

Detection Threshold (DT): Detection threshold is a system design parameter defined as the $S - N$ of the received signal, after processing, at which the SE is zero[33]. In other words, it is the $S - N$ at which the probability of detection (P_d) and probability of false alarm (P_{fa}) are 50%. For an FMCW signal, the optimal detection threshold can be given as follows[33]:

$$DT = 5\log(d) - 10\log BT - 5\log(n) \tag{18}$$

where, d is the detection index, B is the bandwidth of the transmit signal, T is the duration of the signal and n is the number of pings used for signal processing. The detection index, d, is a measure of SNR defined as follows[33]:

$$d = \frac{(mean(S+N) + mean(N))^2}{std\ dev(N)} \tag{19}$$

Now from Eqn. 14 and Eqn. 18, SE for the proposed passive target localization method (with $SINL < N$) becomes:

$$
\begin{aligned}
SE = 159.8 + 10\log(P_{elec}) + G_{Tx} + 10\log(\frac{\lambda^2}{\pi}) \\
+2G_{Bx} - 2PL(d_{Tx\to Bx}, f) + IML_u \\
-PL(d_{Bx\to Target}, f) - PL(d_{Target\to Rx}, f) \\
+TS - N - 5\log(d) - 10\log BT - 5\log(n)
\end{aligned}
\tag{20}
$$

The above equation gives SE as a function of system parameters—such as transducer gains, transmit signal design and operating environment—that can be easily estimated for the informed design of a system.

V. IMPLEMENTATION

A. Experimental components

Our implementation consists of three components:

1. *Transceiver.* A software-defined acoustic modem based on the Raspberry Pi 5 and HiFiBerry DAC+ADC Pro daughterboard (shown in Fig. 8e). Downlink signals produced by the daughterboard's DAC are amplified by a Crown XLi 3500 audio amplifier before being projected by another BT-2RCL transducer (shown in Fig. 8b). Acoustic signals are received by an Aquarian A5 hydrophone, and are recorded by the daughterboard's ADC.

2. *Backscatter Tag.* A piezoelectric backscatter tag (shown in Fig. 8c) consisting of a BTech BT-2RCL transducer and impedance switching circuitry (shown in Fig. 8f) driven by a signal generator at a constant switching frequency. While this switching

implementation is not itself low-power, previous work has demonstrated the feasibility of low-power backscatter switching at similar frequencies[25,34].

3. *Target Object.* A passive acoustic target (rectangular, $30 \times 60 \times 2.5$ cm) fabricated from extruded polystyrene foam (shown in Fig. 8d) mounted with a weight to prevent it from floating.

B. Experimental Setup

Experiments were conducted in a river, with a depth of approximately 5 m. The backscatter tag, projector and hydrophone transducers, and acoustic target were mounted underwater using aluminum extrusion at a depth of 2 m to make the setup rigid against the underwater currents. For all experiments, the projector and hydrophone were placed in a fixed location and approximately collocated, with a spacing of 7 cm. During experiments, a motorized gantry was used to move elements in the water. An example of this experimental setup is shown in Fig. 8a. Unless otherwise noted, for each measurement, the projector transmitted 250-ms-long chirps with a bandwidth of 5 kHz centered at 28 kHz while the backscatter tag switched at a constant rate of 3 kHz. We then processed the received signal in Python with standard signal processing libraries.

VI. EXPERIMENTAL VALIDATION

We performed Backscatter EL (Eqn. 14) verification experiments using the experimental setup described in the previous section. Since the experimental setup was relatively shallow,

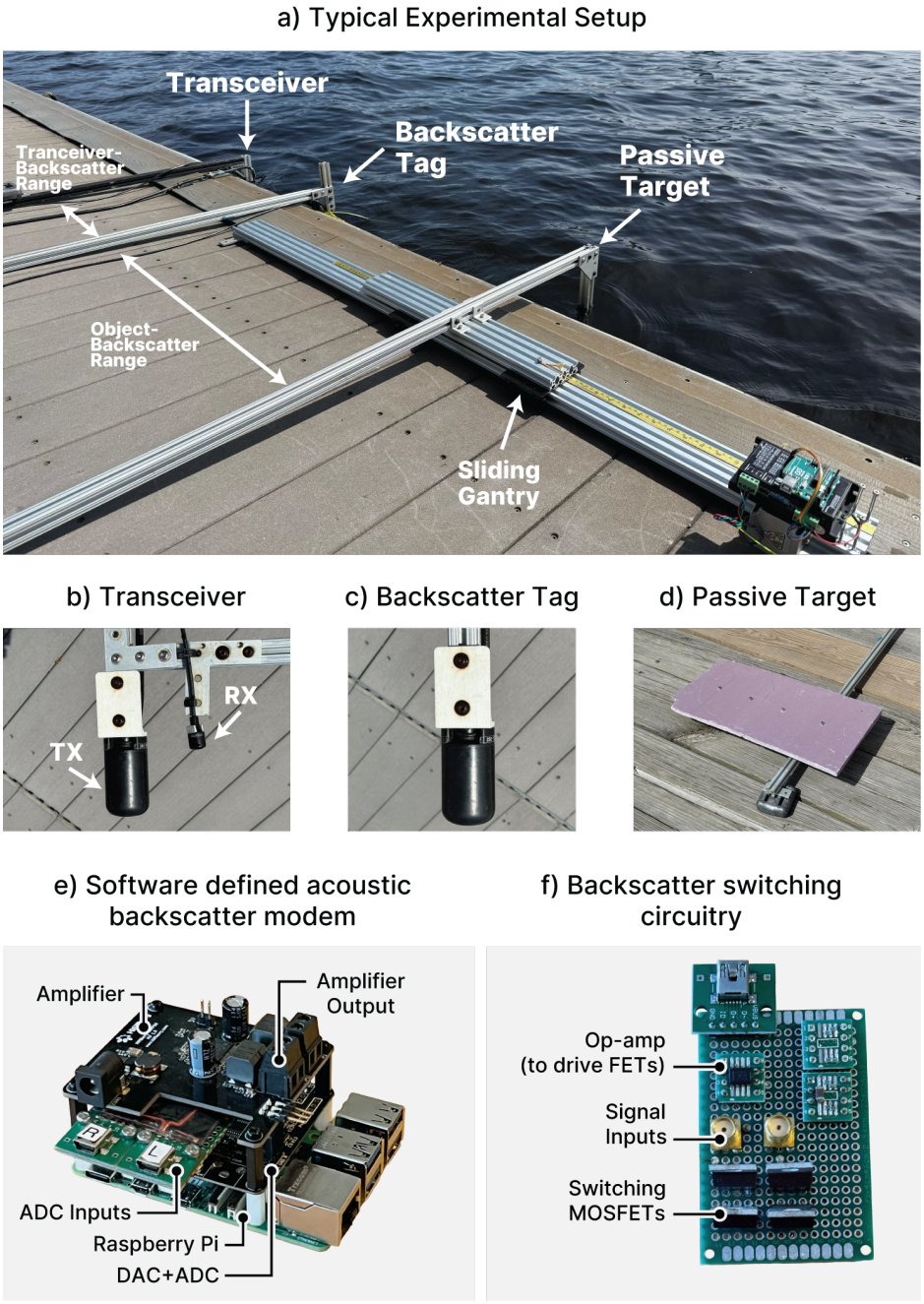

FIG. 8. **Experimental Setup.** In (a), aluminum extrusion was used to mount the transceiver (b), backscatter tag (c), and target (d) at a depth of 2 m. A motorized gantry was used to vary the spacing between acoustic elements. Electronics consisted of a Raspberry Pi-based backscatter modem built around COTS HiFiBerry hardware (e), and switching circuitry for the backscatter tag (f).

we conducted the experiments at short distances, with the maximum distance chosen such that the reflections from the water surface and river bed do not interfere. We made the following measurements:

Source Level (SL) Measurements: To measure the source level of the transmitter, we placed a hydrophone in the far field from the transmitter and measured the received signal strength. We then used the hydrophone's sensitivity to convert the received signal amplitude into the source level. The measured experimental SL was $\sim 158\ dB$.

Backscatter Level (BL) Measurements: To compute the backscatter level, we placed the backscatter tag and the transceiver at a fixed location and then used a hydrophone to measure the received backscatter signal strength at 1 m from the backscatter tag. We then converted this received signal strength into backscatter level using the hydrophone's sensitivity.

Target Strength (TS): To compute the target strength of the object being localized, we transmitted 50 chirps from a transmitter and placed the object at a fixed distance from the transceiver to compute the target strength using the following relation,

$$TS = RL - SL + 2PL(d) \tag{21}$$

We computed the TS by averaging the values at different distances and across 50 chirps. The TS of the board shown in Fig. 8 is measured to be approximately $-5\ dB$.

Channel Reciprocity: We observe that in our experimental setup, with a collocated transmitter and receiver, the two paths (Tx→Bx→Target→Rx and Tx→Target→Bx→Rx) have equal lengths and therefore interfere constructively at the receiver, resulting in a 6 dB gain

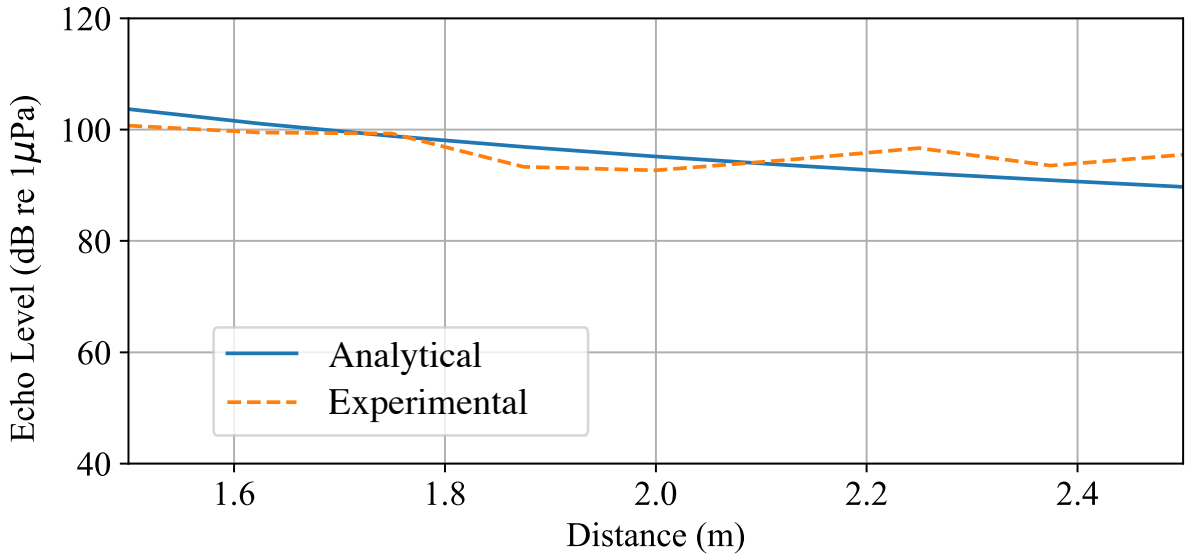

FIG. 9. **Backscatter Echo Level vs. Distance.** The figure plots the distance between the backscatter tag and the target object on the x-axis and backscatter EL on the y-axis. It plots the analytical and experimental results as blue solid and orange dotted curves respectively.

in EL. Thus, we incorporate an additional 6 dB into Eqn. 14 to account for this constructive interference.

We also perform a one-time calibration to account for errors in the sensitivity of the receiver. Next, we use these measurements to experimentally validate the backscatter EL against various parameters, as described in the following sections.

A. Backscatter Echo Level vs. Distance

We validate the backscatter EL against different distances using the experimental setup described before. For these experiments, we fixed the distance between the transceiver and the backscatter tag (1 m) and varied the distance between the target object and the

backscatter tag. Fig. 9 shows the distance between the target object and the backscatter tag on the x-axis and the backscatter EL on the y-axis with the blue curve showing the analytical EL and the orange dotted curve representing the experimental EL. We note that:

1. The backscatter EL predicted by the model accurately traces the measured EL. The error between the model and experimental curves largely remained within $0 - 2\ dB$ with a median deviation of $\sim 0.8\ dB$.

2. The deviations increase at longer distances. This is because, for distances > 2 m, the surface reflection may start to interfere because the water depth and the object's distance from the backscatter tag become comparable. Therefore we limit our experimental analysis to closer distances.

This result validates the analytical model and shows that the model accurately captures the dependence of backscatter EL on varying distances.

B. Backscatter Echo Level vs. Operating Frequency

We next validate the backscatter EL across varying operating frequencies. In the context of an FMCW signal, we define operating frequency to be the center frequency of the chirp. To run these experiments, we fixed the distance between the backscatter tag and the target object to 0.75 m. We then transmitted a signal with fixed bandwidth ($B = 5\ kHz$) and duration ($T = 0.25\ sec$) while sweeping over center frequency from 25 kHz to 31 kHz with an increment of 1 kHz. Fig. 10 plots the center frequency on the x-axis and the backscatter

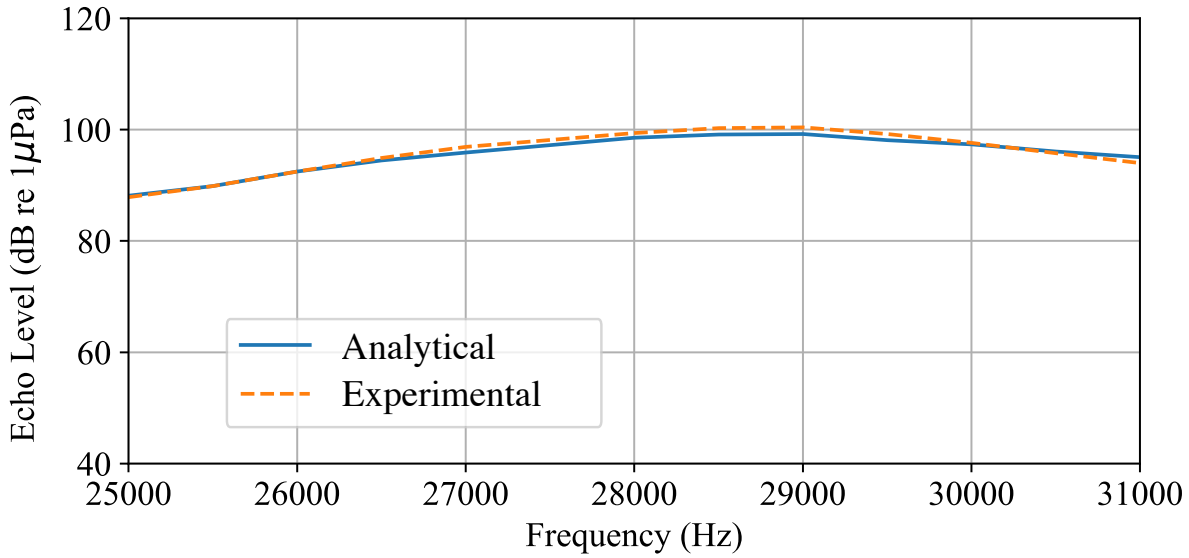

FIG. 10. **Backscatter Echo Level vs. Operating Frequency.** The figure plots the transmitter operating frequency on the x-axis and backscatter EL on the y-axis. It plots the analytical and experimental results as blue solid and orange dotted curves respectively.

EL on the y-axis with the blue solid and orange dotted curves showing the analytical and experimental curves respectively. We note that:

1. The backscatter EL predicted by the model for different center frequencies closely traces the experimental curve, with an error between the experimental and analytical curves of 0–1 dB and a median error of ~ 0.2 dB.

2. The curve also shows approximately 10 dB higher backscatter EL at 28–29 kHz than at a center frequency of 25 kHz. This observation suggests that the optimal region of operation for these types of backscatter tags is around 28 kHz.

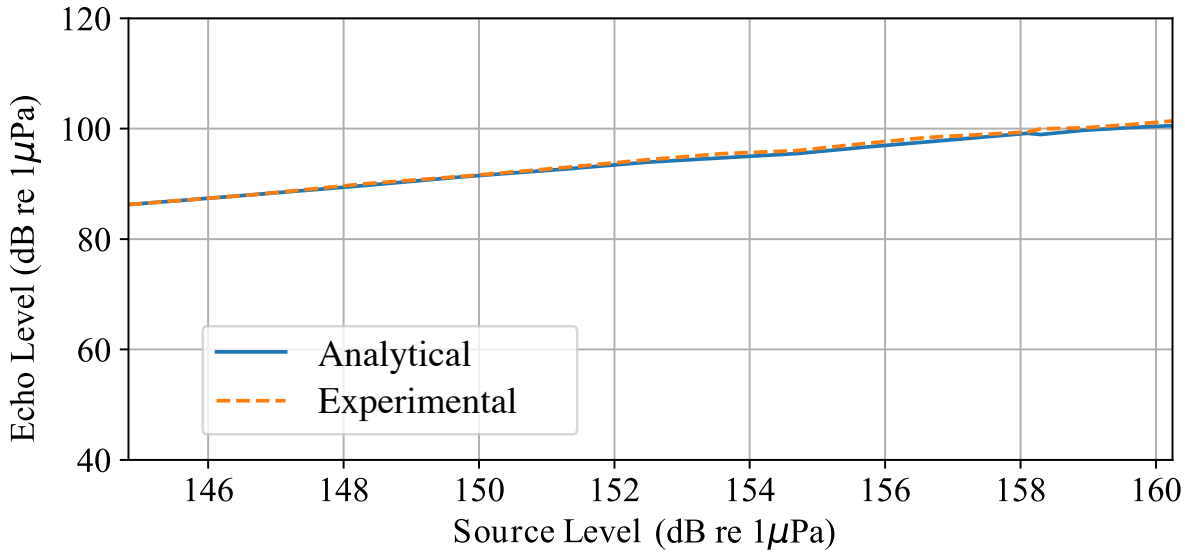

FIG. 11. **Backscatter EL vs Transmitter SL.** The figure plots the transmitter SL on the x-axis and backscatter EL on the y-axis. It plots the analytical and experimental results as blue solid and orange dotted curves respectively.

This result validates our end-to-end analytical model and shows that the model can accurately capture the backscatter performance across operating frequencies.

C. Backscatter Echo Level vs. SL

In this section, we validate the backscatter EL for varying transmitter SL. To do so, we fix the position of the transceiver, the backscatter tag, and the target object at the distances mentioned in the previous sections. We then vary the SL of the transmitter by changing the input power of the transmitter and measure the input SL using a receiver placed in the far field (1.75 m) from the transmitter. We then plot the experimentally determined backscatter EL and compare it with the analytical results. Fig. 11 shows the input SL on the

x-axis and backscatter EL on the y-axis with blue solid and orange dotted curves showing the analytical and experimental results respectively. We note that:

1. As expected, increasing the input source level increases the backscatter EL as well. The analytical and experimental curves trace each other well, with a median deviation of approximately 0.4 dB.

2. The linear increase in backscatter EL with source level suggests that the effective localization range can, in principle, be extended by increasing the source level. This insight is important because it indicates that the operational range of the system can be controlled in a predictable manner through the transmitter.

This experimental validation suggests that our end-to-end analytical model accurately captures the performance of the proposed localization method across varying transmitter SL.

VII. LOCALIZATION RESULTS

A. One-Dimensional Localization Results

To evaluate the one-dimensional passive target localization performance via a single backscatter tag, we place the tag at a fixed distance of 50 cm from the TRx and position the target object (collinear with the transceiver and the backscatter tag) at different distances from the tag. Ground truth distances were produced with the sliding gantry, and confirmed with a tape measure. We observe that for the given system parameters (SL, transducer gains, noise level, TS, etc.) the maximum distance at which the backscatter EL

could be recorded was 4.0 m, beyond which the signal was buried in the noise. We then collected measurements for different target distances up to 4.0 m from the backscatter tag. We then estimated the object location from the backscatter tag using the algorithm described in §III and measured the localization error. We used $n = 3$ chirps for distance estimation and repeated the measurement 16 times at each distance. We then plot the cumulative distribution function (CDF) of the one-dimensional localization error as shown in Fig. 12 with the CDF on the y-axis and localization error on the x-axis. Note that:

1. The plot shows the 50th and 90th percentile errors of 6.4 cm and 14 cm respectively.

2. Recall that we use a 5 kHz chirp, which yields a range resolution[35] of approximately 15 cm. This is consistent with the localization error shown in Fig. 12.

This result shows that a single backscatter tag can be used to accurately determine the distance of a reflector, indicating the feasibility of the proposed method.

B. Two-Dimensional Localization Accuracy

1. Quantitative Results

In this section, we present results for two-dimensional localization. We ran experiments as described in the previous section, but this time we used multiple backscatter tag locations (not necessarily collinear) for geometric diversity. The tag locations for 1, 3, and 9 tags are shown in Fig. 13b. We performed background subtraction to eliminate surface reflections and estimated distances by processing three chirps.

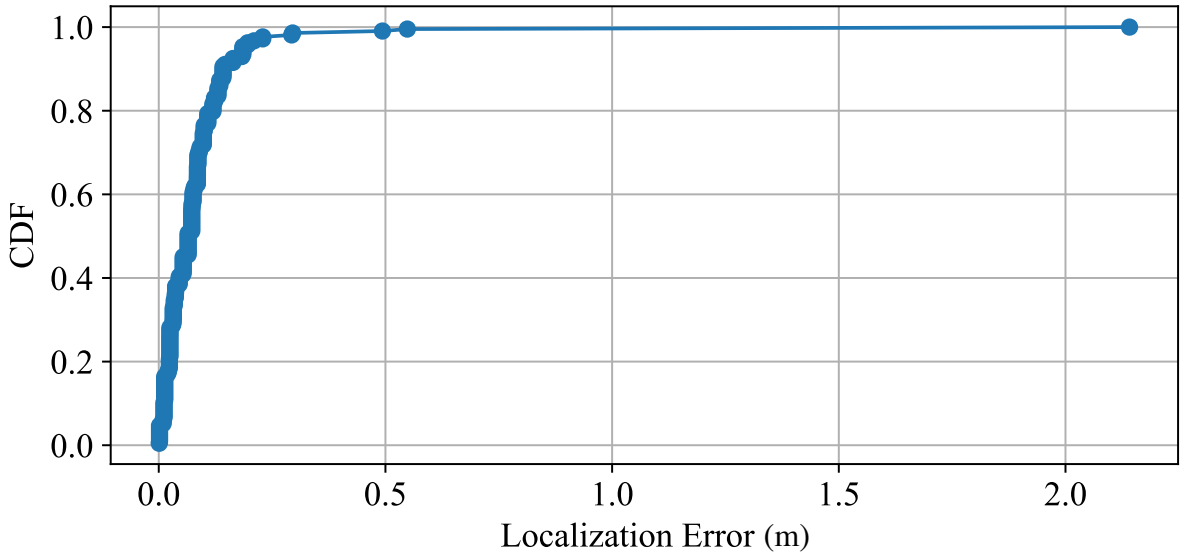

FIG. 12. **Cumulative distribution function (CDF) of one-dimensional localization.** The figure plots the one-dimensional localization error on the x-axis and CDF on the y-axis.

These distance estimates were then used to construct a probability map of the target's location. From this map, we estimated the target position and compared it with the ground truth to measure localization error. Fig. 13a plots the CDF of the two-dimensional localization error. The figure shows three curves corresponding to the CDF of the 2D localization error when using one (blue), three (orange), and nine (green) backscatter tag positions. Specifically, to construct the blue curve, we used the tag location marked as 1 in Fig. 13b. Similarly, for the orange curve, we used three backscatter tags placed at locations marked as 1, 2, and 3 in Fig. 13b with switching rates of 5, 4, and 3 kHz, respectively and for the green curve, we emulated a larger array of nine tags by moving a single tag (switching at 3 kHz) through nine tag locations for location estimation. Note that:

1. The results show the superior performance of the two-dimensional localization when using 9 backscatter tags over configurations with 3 and 1 backscatter tags with 90th-percentile errors of 0.6 m, 2.2 m and 7.2 m respectively.

2. The results also show better median performance as the number of backscatter tags increases, with localization errors of 7.9 cm, 19 cm, and 2.0 m at the 50th percentile for 9, 3, and 1 backscatter tags, respectively.

3. In the presence of only a single backscatter tag, geometric diversity is limited. As a result, although the tag can estimate range accurately with an average localization error of 4.5 cm, two-dimensional localization suffers from the lack of sufficient viewpoints.

These results demonstrate that increasing the number of backscatter tag positions improves geometric diversity and, consequently, two-dimensional localization accuracy.

2. Qualitative Results

We also qualitatively evaluate how increasing the number of tags affects two-dimensional localization estimates. Fig. 14 and Fig. 15 show the normalized two-dimensional localization probability heatmaps for various backscatter locations. The purple rectangle in all the figures represents the ground-truth location of the target object, and the red dots represent the different backscatter tag positions. The figure also identifies the TRx; the depicted Tx and Rx dimensions are not to scale. In Fig. 14, we compare heatmaps produced when using different sizes of backscatter arrays (i.e., different number of backscatter tag locations),

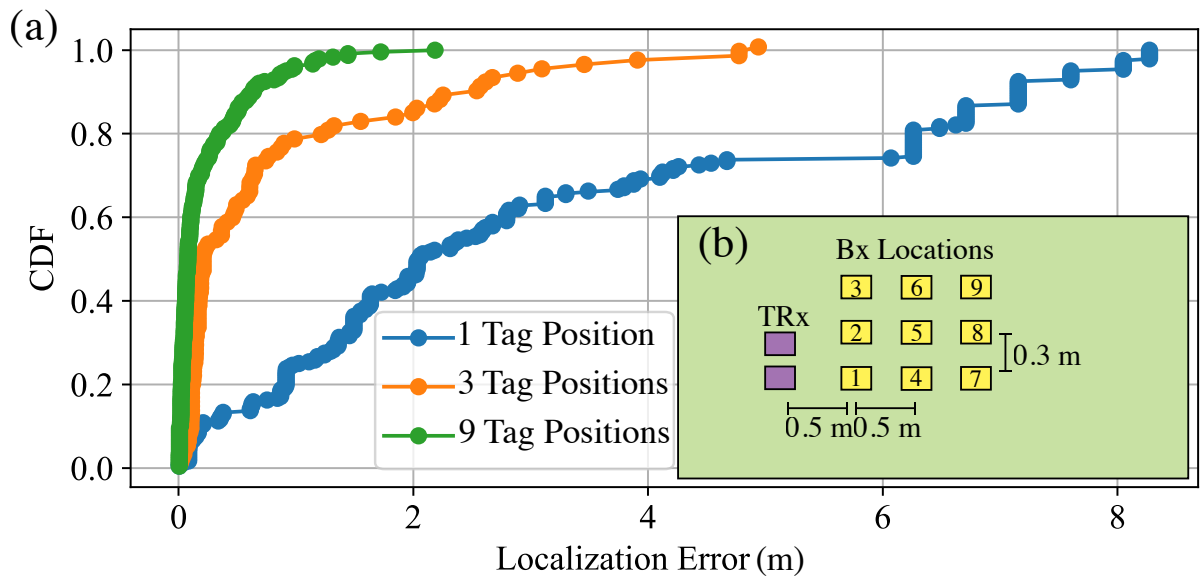

FIG. 13. **CDF of 2-D Localization.** a) plots the CDF of 2D localization results when using one, three, and nine backscatter tag locations for spatial diversity as blue, orange, and green curves respectively. b) shows the backscatter tag locations (as numbered yellow box) with respect to the transceiver (purple box).

whereas Fig. 15 compares the effect of the backscatter array distance to the object. We make the following remarks:

1. In Fig. 14, although the heatmaps assign high probability to the true target location in all cases, the localization resolution improves as the number of backscatter tags increases. This is because the number of tags is directly related to the number of vantage points for localization.

2. As evident from Fig. 15, the localization resolution not only depends on the number of vantage points but is also impacted by their distance to the target object. Specifically,

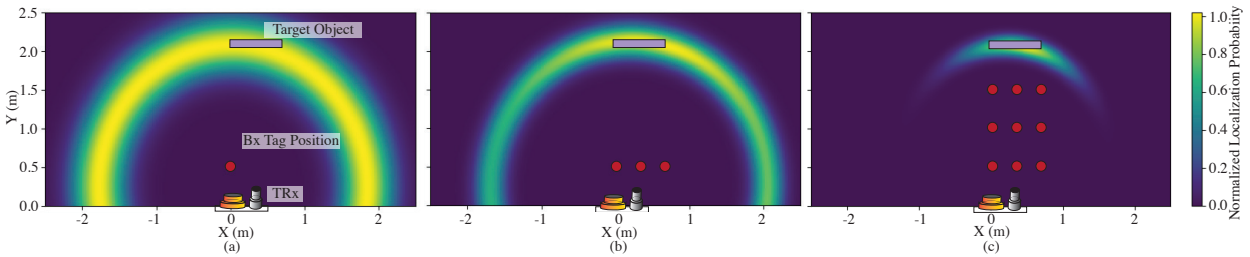

FIG. 14. **Varying Number of Backscatter Tags.** The figure shows the heatmap of the passive target localization when using a) one, b) three, and c) nine backscatter tag locations.

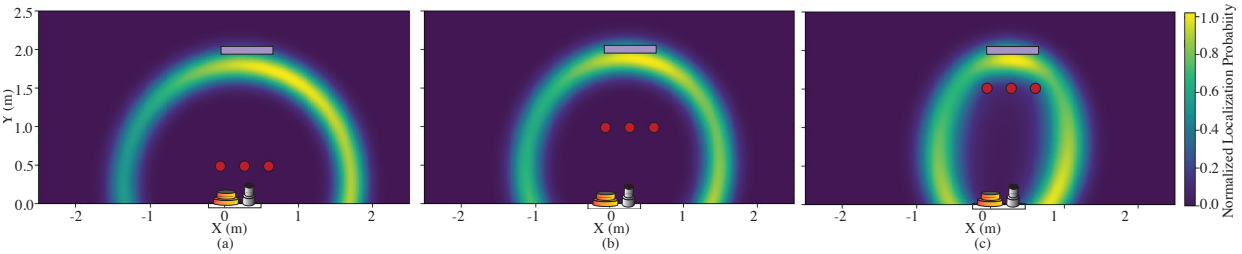

FIG. 15. **Varying Backscatter-Target Distances.** The figure shows heatmaps of passive target localization using three backscatter tags at backscatter-tag-to-target distances of (a) 1.5 m, (b) 1.0 m, and (c) 0.5 m.

when the tags are closer to the target object (Fig. 15c) they provide higher geometric diversity with respect to the target object as compared to when they are further from the target (Fig. 15a). This result shows that as the target object moves away from the surface, the proposed method can be used to build arrays that can be moved closer to the target object to provide better localization resolution, without moving the transceiver deployed in a power-privileged location.

These heatmaps show that both the number and placement of backscatter tags play a role in improving two-dimensional localization resolution.

VIII. DESIGN TRADEOFFS AND PERFORMANCE ANALYSIS

In the previous sections, we experimentally validated the backscatter EL model and presented initial localization results. In this section, we use the validated model to analyze key design tradeoffs and quantify the impact of various system and environmental parameters on the performance of the proposed method. System performance is characterized by two complementary metrics: localization range and localization resolution. These metrics should be considered separately because they impose different, and sometimes competing, requirements on backscatter-tag placement. We therefore first analyze the achievable localization range while holding the localization geometry fixed, and then evaluate localization resolution under the assumption that the target echoes remain detectable.

A. Localization Range Analysis

To study the impact of various design parameters on localization range, we plot the maximum target detection distance as a function of transmitter SL. As mentioned earlier, for localization range analysis we hold the resolution constant. To do so, we fix the distance between the backscatter tag and the target object. Specifically, unless otherwise specified, we fix the distance between the backscatter tag and target to be 5 m. Similarly, we set the backscatter tag gain (G_{tag}) to be $0dB$, impedance mismatch loss ($IMLu$) to be 0, target strength (TS) to be -10 dB, spreading factor (k) to be 2, and noise density (N) to be 60 dB, corresponding to a moderate ambient noise regime[36]. We then compute the localization range as the maximum distance that satisfies $EL = N+DT$, where the detection

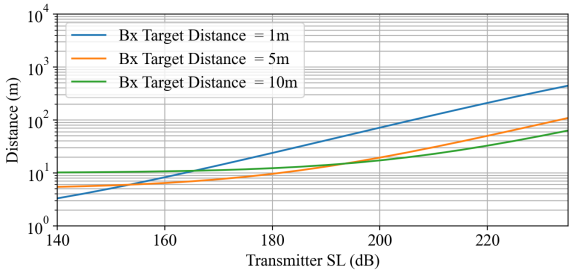

(a) Localization range versus transmitter source level for varying transceiver-to-tag distances.

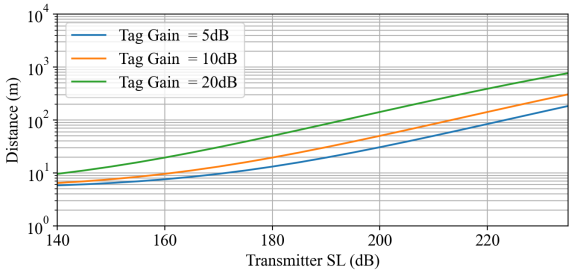

(b) Localization range versus transmitter source level for varying backscatter tag gains.

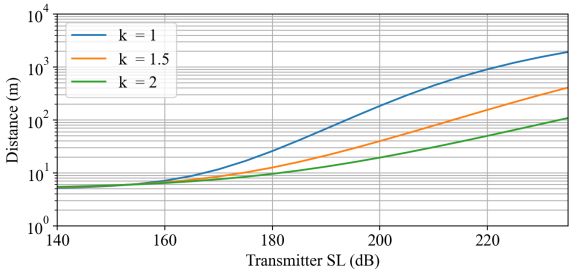

(c) Localization range versus transmitter source level for varying spreading factors.

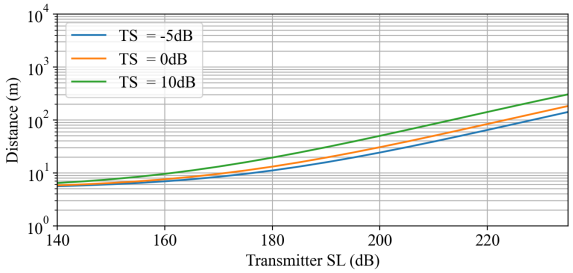

(d) Localization range versus transmitter source level for varying target strengths.

FIG. 16. **Localization Range Under Different System and Environmental Parameters.**

threshold DT is calculated using Eqn. 18 with $n = 1$, $B = 5000\ Hz$, and $T = 0.25$ s. We use $5 \log d = 8$ for a broadband signal with $P_{fa} = 10^{-5}$ and $P_d = 0.9$[33].

Impact of the Backscatter-Target Distance. Assuming the collinear geometry in §VI, Fig. 16a plots the maximum detection distance versus transmitter source level for $d_{Bx \to Target} = 1$ m, 5 m, and 10 m. Note that since the backscatter-to-target distance directly affects localization resolution, the three curves correspond to different resolution regimes, while the resolution remains fixed along each individual curve. At $d_{Bx \to Target} = 1$ m, an SL of $\sim 235\ dB\ re\ \mu Pa$[37] supports a detection range of about 420 m at minimal backscatter gain

of 0 dB and an object of $TS = -10$ dB. Increasing the backscatter-tag-to-target distance from 1 m to 5 m decreases the detection range to about 120 m at the same system settings. Increasing the backscatter-tag-to-target distance weakens the backscatter EL because of the additional path loss; however, comparable performance can be achieved by increasing the transmitter SL and/or backscatter tag gain.

Impact of Backscatter Tag Gain. Since the tag gain G_{Bx} contributes directly to SE in Eqn. 20, increasing the tag gain can improve the detection range of the system. Tag gain can be increased through a larger physical aperture, an array of elements, or low-power amplification[38–41]. Fig. 16b plots range versus transmitter SL for tag gains of 5, 10, and 20 dB, using the previous setup with the $d_{Tx \to Bx} = 5$ m. The plot shows that a tag gain of 5 dB increases the range to about 200 m at an SL of $\sim$ 235 $dB\ re\ \mu Pa$. Similarly, a tag gain of 20 dB further increases the range to about 800 m.

Impact of Spreading Factor. Environmental factors like spreading factor also have a direct impact on the range of the system. Loss scales quadratically with distance for spherical spreading ($k = 2$) and linearly for cylindrical spreading ($k = 1$). In practice, the spreading factor falls between these values, depending on the water's depth and environmental conditions[42]. Fig. 16c compares $k = 1$, 1.5, and 2 for $G_{tag} = 0$, $TS = -10$ dB, $d_{Bx \to Target} = 5$ m, and $IMLu = 0$. The plot shows that in a narrow channel ($k = 1$), the system range reaches 1.8 km, compared with 120 m at an SL of $\sim$ 235 $dB\ re\ \mu Pa$ and $k = 2$. The $k = 1$ curve bends at long range as absorption becomes significant, illustrating the strong environmental impact on range.

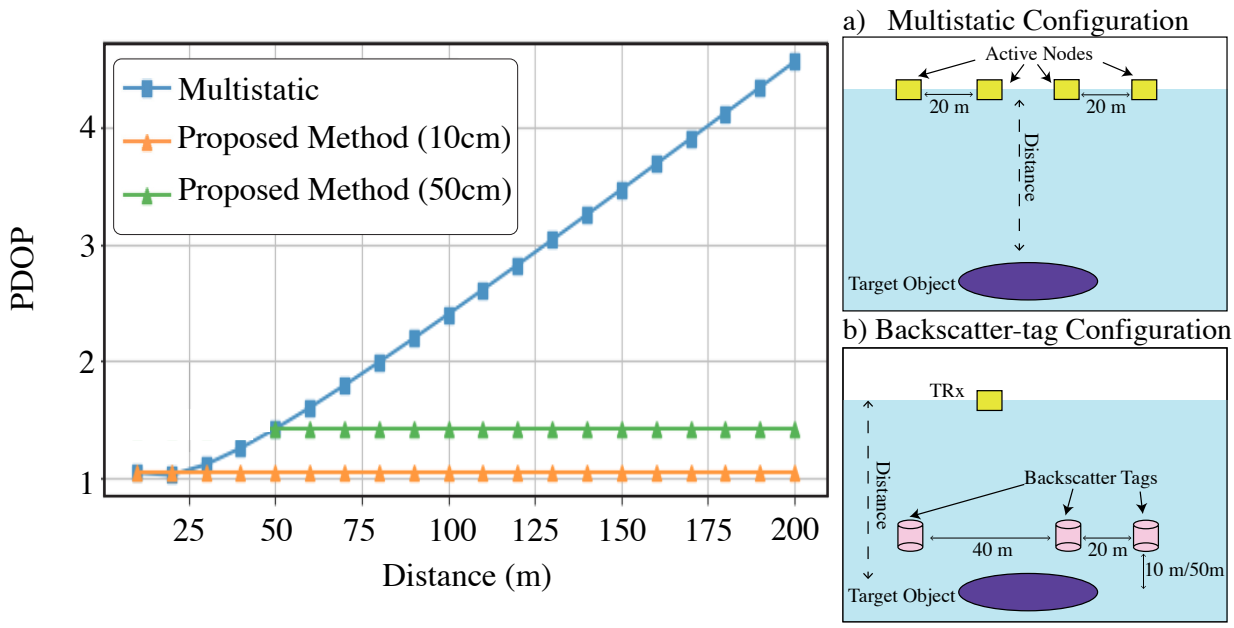

FIG. 17. **PDOP vs. Distance of the Target from the Transceiver.** The figure plots PDOP as a function of the target's distance from the transceiver.

Impact of Object TS. Fig. 16d compares ranges for $TS = -5$, 0, and 10 dB under the same conditions. Target strength depends on shape, size, and material; for example, an underwater vehicle can have an average target strength of about 20 dB[43], while a 2 m sphere is about 0 dB[33]. At SL of 235 $dB\ re\ \mu Pa$, a target with $TS = -5$ dB yields about 140 m of range, while one with $TS = 10$ dB yields roughly twice that range. Thus, stronger reflectors naturally enable greater localization ranges, reducing the burden on the system to extend detection range in applications involving highly reflective targets.

B. Localization Resolution Analysis

Thus far, we have examined how various system and environmental parameters affect the detectability of the backscatter EL without focusing on the placement of the backscatter

tags for geometric diversity. In this section, we quantitatively evaluate how the placement of the backscatter tags affects localization accuracy. Note that, because the analysis in this section focuses on localization resolution, we assume that the backscatter tags operate within the detection range of the system.

To quantify localization accuracy, we use the Position Dilution of Precision (PDOP) metric commonly employed in GPS. PDOP characterizes how the geometry of localization anchors (satellites in the case of GPS) affects the localization accuracy at the receiver, with a higher PDOP indicating greater localization error. Mathematically, PDOP can be written as:

$$\text{PDOP} = \sqrt{\sigma_x^2 + \sigma_y^2 + \sigma_z^2}, \tag{22}$$

where σ_x^2, σ_y^2, and σ_z^2 are the variances of the measurement errors in x, y, and z dimensions, respectively. These are the diagonal elements of the positional covariance matrix $\mathbf{Q}$ defined as,

$$\mathbf{Q} = \left(\mathbf{G}^T\mathbf{G}\right)^{-1}. \tag{23}$$

where $\mathbf{G}$ is the geometry matrix defined as follows:

$$\mathbf{G} = \begin{bmatrix} \frac{x-x_1}{r_1} & \frac{y-y_1}{r_1} & \frac{z-z_1}{r_1} & 1 \\ \frac{x-x_2}{r_2} & \frac{y-y_2}{r_2} & \frac{z-z_2}{r_2} & 1 \\ \vdots & \vdots & \vdots & \vdots \\ \frac{x-x_N}{r_N} & \frac{y-y_N}{r_N} & \frac{z-z_N}{r_N} & 1 \end{bmatrix}, \tag{24}$$

Where (x_i, y_i, z_i) is the location of the ith reference node and (x, y, z) is the location of the target. r_i is the distance between the target and the ith node and N is the number of reference nodes.

Because there are infinitely many possible tag-placement configurations, each with a different localization resolution, we restrict our analysis to a two-dimensional setting in which the backscatter tags are placed along a line and only the distance between each tag and the target is varied. Fig. 17 compares the PDOP achieved by the proposed method with that of a surface-borne multistatic configuration used as the baseline by plotting the PDOP on the y-axis and the distance of the target from the transceiver on the x-axis. Since PDOP depends on many factors including the number and location of the vantage points and their relative distance from the target, to simplify the analysis we assume a two-dimensional setting with the following configurations:

Multistatic Configuration. We assume four floating nodes ($N = 4$) spaced 20 m apart as shown in Fig. 17a. The PDOP against the distance for this configuration is shown as blue curve in Fig. 17.

Backscatter-tag Configuration. We fix the total number of nodes to be four (one transceiver and 3 backscatter tags) with the same horizontal spacing as in the multistatic configuration. Since the benefit of the proposed method comes from the fact that the backscatter tags can be moved closer to the target object to provide the geometric diversity, for the purposes of this analysis we fix the vertical distance between the backscatter tag and the target. This configuration is shown in Fig. 17b. We plot the results for two backscatter-

target distances i.e., 10 m and 50 m. The PDOP for these two configurations are plotted as orange and green curves respectively in Fig. 17.

Note that,

- As the distance between the target and the active transmitter increases, the PDOP of the multistatic configuration increases approximately linearly. Specifically, the PDOP increases from 1.0 at 10 m to 4.5 at approximately 200 m. This increase occurs because the geometric diversity decreases as the target moves farther from the array, resulting in lower localization accuracy.

- For the backscatter-tag configuration, the PDOP remains nearly constant as the target moves farther from the active transmitter. This behavior is expected because, in the proposed method, the geometric diversity is determined by the locations of the backscatter tags. Consequently, localization accuracy depends primarily on the tag placement rather than on the distance between the target and the active transmitter.

- Note that as the distance between the backscatter tag and target changes from 10 m to 50 m, the PDOP changes from ~ 1 to ~ 1.4 (orange and green plot respectively) indicating that for fixed inter-tag distance, as we move tags farther away from the object, the localization resolution begins to degrade.

IX. THEORETICAL EXTENSIONS

Building on these results, this article demonstrates how backscatter tags distributed in the environment can be leveraged to localize passive targets without increasing power

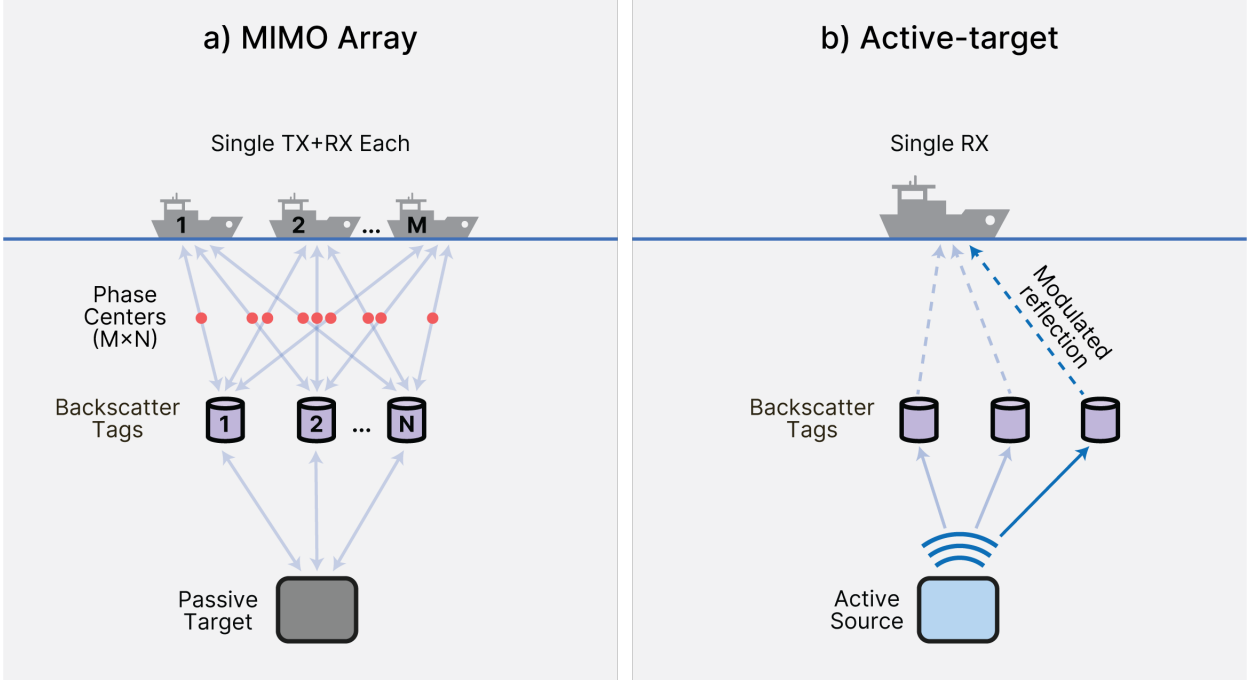

FIG. 18. **Backscatter Localization Extensions.** (a) shows how an array of M transceivers and N backscatter tags can produce an $M \times N$ virtual receiver array. (b) shows that an active acoustic source can provide the carrier signal for backscatter modulation and enable localization.

consumption, cost, or deployment complexity. In this section, we discuss several potential extensions of this work, focusing on different configurations in which backscatter tags can further enhance localization performance and enable new applications.

MIMO Configuration: A promising direction for future work is to extend this framework to configurations with multiple transceiver locations. This could be realized either by moving a single transceiver across M locations or by deploying M distinct transceivers, as shown in Fig. 18a. In such a setting, the presence of backscatter tags could further enhance system performance by introducing an additional array gain. Specifically, similar to MIMO radar imaging[44], the backscatter tags may be viewed as transmitters and the M transceivers as

receivers[45]. This configuration would create an $M \times N$-element virtual array, whose elements are located at the phase centers of each backscatter tag–transceiver pair. As a result, the virtual array could provide an aperture gain proportional to $M \times N$. Notably, this gain would come in addition to the original M-fold array gain provided by the M transceivers themselves. Consequently, such a MIMO configuration could in principle yield an overall gain that scales as M^2N.

Active Target Localization: A promising direction for future work is to extend this framework to active target localization. Unlike the passive target localization scenario considered in this article, in this case the target itself transmits the signal of interest, and there is no dedicated transmitter elsewhere in the system. As shown in Fig. 18b, the backscatter tags could still provide geometric diversity by increasing the number of vantage points, even though they would now be excited by the unknown signal emitted by the target itself. In principle, the signals backscattered by different tags could be separated and then used to localize the target, similar to prior work[4], by exploiting their relative delays for elliptical multilateration.

MIMO Configuration in Active Target Localization: Similar to the MIMO configuration described earlier in this section, a natural extension to active target localization would be to consider a MIMO configuration with M transceiver locations and N backscatter tags in the environment. In principle, this would provide an M-element receiver-array gain across the N backscatter tags, resulting in an overall gain proportional to $M \times N$.

Overall, these extensions suggest that the use of backscatter tags is not limited to the passive localization scenario considered in this article. Rather, they point to a broader design

space in which backscatter tags can provide geometric diversity and array gain across different sensing configurations. Developing these extensions more fully remains an important direction for future work.

X. CONCLUSION

This article presented a passive target localization method that uses spatially distributed acoustic backscatter tags to increase geometric diversity while requiring only a single acoustic transceiver. By treating the backscatter tags as controllable secondary reflectors, the proposed approach provides an alternative to conventional multistatic configurations that would otherwise require multiple active nodes and the associated increases in power consumption, cost, and deployment complexity. To analyze this system, we developed a closed-form end-to-end analytical model for passive target localization by extending classical echo-level analysis to account for the electro-acoustic behavior of underwater backscatter tags. Experimental validation in a river environment showed close agreement between the analytical model and measurements, with median deviations of 0.8 dB, 0.2 dB, and 0.4 dB across varying target distances, operating frequencies, and transmitter source levels, respectively. We also demonstrated a proof-of-concept prototype and showed that the proposed method can achieve a median one-dimensional localization error of 6.4 cm, while two-dimensional localization improves substantially as the number of backscatter-tag vantage points increases, reaching median and 90th-percentile errors of 7.9 cm and 0.6 m, respectively, when nine tag positions are used. Finally, the validated model was used to study key design tradeoffs, including transceiver-to-tag distance, tag gain, spreading conditions, and target strength,

and to examine how these parameters affect achievable localization range. Taken together, these results show that acoustic backscatter tags can serve not only as ultra-low-power communication devices, but also as a practical mechanism for improving passive underwater localization.

XI. AUTHOR DECLARATION

This research was supported by the Office of Naval Research under ONR Grant No. N00014-23-1-2838-P00002.

A. Conflict of Interest

The authors have no conflicts to disclose.

B. Data Availability

Data supporting the findings of this article are available upon request.

REFERENCES

[1]P. Batista, C. Silvestre, and P. Oliveira, "A sensor-based long baseline position and velocity navigation filter for underwater vehicles," IFAC Proceedings Volumes **43**(14), 302–307 (2010).

[2]X. Su, I. Ullah, X. Liu, and D. Choi, "A review of underwater localization techniques, algorithms, and challenges," Journal of Sensors **2020** (2020).

[3]J. Opderbecke, "At-sea calibration of a usbl underwater vehicle positioning system," in *Oceans' 97. MTS/IEEE Conference Proceedings*, IEEE (1997), Vol. 1, pp. 721–726.

[4]Z. Yang, Z. Zhu, Y. Zhao, Y. Tian, C. Fan, R. Guo, W. Lu, J. Ge, B. Chen, Y. Zhang, G. Wu, R. Wang, G. Eigner, G. Cheng, J. Huang, Z. Liu, J. Zhang, I. J. Rudas, and F.-Y. Wang, "A comprehensive survey on underwater acoustic target positioning and tracking: Progress, challenges, and perspectives" (2025), https://arxiv.org/abs/2506.14165.

[5]V. E. Premus, P. A. Abbot, E. Illich, T. A. Abbot, J. Browning, and V. Kmelnitsky, "North atlantic right whale detection range performance quantification on a bottom-mounted linear hydrophone array using a calibrated acoustic source," The Journal of the Acoustical Society of America **158**(5), 3672–3686 (2025) https://doi.org/10.1121/10.0039669 doi: 10.1121/10.0039669.

[6]L. Jia, G. Zhang, Y. Liu, Z. Bai, Y. Geng, Y. Wu, J. Zhang, and W. Zhang, "Sonar buoy active detection and localization for underwater targets using high-level sound sources and mems hydrophone," Measurement **241**, 115740 (2025).

[7]A. Zhao, L. Ma, J. Hui, and L. Liu, "Research and implementation of bistatic sonar positioning system based on vector hydrophone," in *2016 IEEE/OES China Ocean Acoustics (COA)*, IEEE (2016), pp. 1–5.

[8]J. Marszal and R. Salamon, "Silent sonar for maritime security applications," in *Proceedings of Meetings on Acoustics*, Acoustical Society of America (2012), Vol. 17, p. 070082.

[9]J. Dillon and R. Charron, "Resolution measurement for synthetic aperture sonar," in *OCEANS 2019 MTS/IEEE SEATTLE* (2019), pp. 1–6, doi: 10.23919/OCEANS40490.2019.8962823.

[10]L. Fu, M. Zhou, L. Xu, X. Dong, Z. Kou, and C. Kang, "Effective deployment strategies for optimizing area coverage in multistatic sonar detection based on cassini oval approximation and a virtual force algorithm," Ain Shams Engineering Journal **15**(12), 103147 (2024) https://www.sciencedirect.com/science/article/pii/S2090447924005288 doi: https://doi.org/10.1016/j.asej.2024.103147.

[11]S. Kim, B. Ku, W. Hong, and H. Ko, "Performance comparison of target localization for active sonar systems," IEEE transactions on aerospace and electronic systems **44**(4), 1371–1380 (2009).

[12]K. Zhao, J. Liang, J. Karlsson, and J. Li, "Enhanced multistatic active sonar signal processing," The Journal of the Acoustical Society of America **134**(1), 300–311 (2013).

[13]D. J. Peters, "A bayesian method for localization by multistatic active sonar," IEEE Journal of Oceanic Engineering **42**(1), 135–142 (2016).

[14]F. Ehlers, M. Daun, and M. Ulmke, "System design and fusion techniques for multistatic active sonar," in *OCEANS 2009-EUROPE*, IEEE (2009), pp. 1–10.

[15]S. Yildiz, P. Roux, S. T. Rakotonarivo, C. Marandet, and W. Kuperman, "Target localization through a data-based sensitivity kernel: A perturbation approach applied to a multistatic configuration," The Journal of the Acoustical Society of America **135**(4), 1800–1807 (2014).

[16]J. Liu, Z. Zhou, and X. Zeng, "Research on multi-static active sonar target recognition based on machine learning," in *2019 3rd International Conference on Electronic Information Technology and Computer Engineering (EITCE)*, IEEE (2019), pp. 1921–1925.

[17]J. Jang and F. Adib, "Underwater backscatter networking," in *Proceedings of the ACM special interest group on data communication*, pp. 187–199.

[18]S. S. Afzal, W. Chen, and F. Adib, "3d-blue: Backscatter localization for underwater robotics," in *2024 IEEE/RSJ International Conference on Intelligent Robots and Systems (IROS)*, IEEE (2024), pp. 11040–11047.

[19]A. Eid, J. Rademacher, W. Akbar, P. Wang, A. Allam, and F. Adib, "Enabling long-range underwater backscatter via van atta acoustic networks," in *Proceedings of the ACM SIGCOMM 2023 Conference*, ACM SIGCOMM '23, Association for Computing Machinery, New York, NY, USA (2023), p. 1–19, https://doi.org/10.1145/3603269.3604814, doi: 10.1145/3603269.3604814.

[20]W. Akbar, A. Allam, and F. Adib, "The underwater backscatter channel: Theory, link budget, and experimental validation," in *Proceedings of the 29th Annual International*

Conference on Mobile Computing and Networking (2023), pp. 1–15.

[21]W. Akbar, A. Allam, and F. Adib, "Underwater backscatter networking for subsea iot: A link-budget analysis in practical ocean channels," IEEE Journal of Oceanic Engineering **50**(3), 1703–1717 (2025).

[22]A. Bhardwaj, A. Erturk, and K. G. Sabra, "Broadband wireless battery-free acoustic identification tags for high data-rate underwater backscatter communication," The Journal of the Acoustical Society of America **157**(1), 445–458 (2025).

[23]S. S. Afzal, W. Akbar, O. Rodriguez, M. Doumet, U. Ha, R. Ghaffarivardavagh, and F. Adib, "Battery-free wireless imaging of underwater environments," Nature communications **13**(1), 5546 (2022).

[24]S. S. Afzal, J. Rademacher, W. Chen, P. Wang, and F. Adib, "Scalable and low power localization for underwater robots," in *Proceedings of the 31st Annual International Conference on Mobile Computing and Networking* (2025), pp. 1075–1090.

[25]N. Naeem, J. Rademacher, R. Patnaik, T. Boroushaki, and F. Adib, "Seascan: An energy-efficient underwater camera for wireless 3d color imaging," in *Proceedings of the 30th Annual International Conference on Mobile Computing and Networking* (2024), pp. 785–799.

[26]S. J. Lourey and J. Lau, "Continuous active sonar tracking and correlated measurements," Proceedings of Meetings on Acoustics **44**(1), 055002 (2021) https://doi.org/10.1121/2.0001465 doi: 10.1121/2.0001465.

[27]A. Meta, P. Hoogeboom, and L. P. Ligthart, "Signal processing for fmcw sar," IEEE Transactions on geoscience and remote sensing **45**(11), 3519–3532 (2007).

[28]G. Hickman and J. L. Krolik, "Non-recurrent wideband continuous active sonar," in *2012 Oceans*, IEEE (2012), pp. 1–6.

[29]S. M. Murphy, L. M. Zurk, and M. E. Coffin, "Processing continuous active sonar transmissions to achieve an arbitrarily fast update rate with full instantaneous bandwidth," IEEE Journal of Oceanic Engineering **46**(3), 988–999 (2020).

[30]S. J. Lourey, "Frequency hopping waveforms for continuous active sonar," in *2015 IEEE International Conference on Acoustics, Speech and Signal Processing (ICASSP)*, IEEE (2015), pp. 1832–1835.

[31]D. A. Hague and J. R. Buck, "The generalized sinusoidal frequency-modulated waveform for active sonar," IEEE Journal of Oceanic Engineering **42**(1), 109–123 (2016).

[32]When processing in the complex signal domain, the copies of the backscatter signal (also shown in Fig. 5a) appear in the negative side of the spectrum as well.

[33]A. D. Waite, *Sonar for Practising Engineers*, 3rd ed. (Wiley, 2002).

[34]R. Menon, J. Rademacher, and F. Adib, "Leveraging underwater backscatter for long-term environmental sensing," in *Proceedings of the 31st Annual International Conference on Mobile Computing and Networking* (2025), pp. 1204–1206.

[35]The range resolution is given by $r = \frac{c}{2B}$, where c is the speed of sound, B is the signal bandwidth, and r is the resulting range resolution.

[36]J. M. Sills, B. L. Southall, and C. Reichmuth, "The influence of temporally varying noise from seismic air guns on the detection of underwater sounds by seals," The Journal of the Acoustical Society of America **141**(2), 996–1008 (2017).

[37]Naval SONAR often has a source level that falls between 220–235 $dB\ re\ \mu Pa$[46].

[38]F. Amato, C. W. Peterson, M. B. Akbar, and G. D. Durgin, "Long range and low powered rfid tags with tunnel diode," in *2015 IEEE International Conference on RFID Technology and Applications (RFID-TA)*, IEEE (2015), pp. 182–187.

[39]F. Amato, C. W. Peterson, B. P. Degnan, and G. D. Durgin, "Tunneling rfid tags for long-range and low-power microwave applications," IEEE Journal of Radio Frequency Identification **2**(2), 93–103 (2018).

[40]F. Amato and G. D. Durgin, "Tunnel diodes for backscattering communications," in *2018 2nd URSI Atlantic Radio Science Meeting (AT-RASC)*, IEEE (2018), pp. 1–3.

[41]F. Amato, "Achieving hundreds-meter ranges in low powered rfid systems with quantum tunneling tags," Ph.D. thesis, Georgia Institute of Technology, 2017.

[42]J. Preisig, "Acoustic propagation considerations for underwater acoustic communications network development," ACM SIGMOBILE Mobile Computing and Communications Review **11**(4), 2–10 (2007).

[43]C. R. Andriani, "Submarine target strength estimates at 1 khz," DTIC Technical Report AD0531451, Naval Research Laboratory, Washington, D.C. (1974), https://apps.dtic.mil/sti/citations/AD0531451.

[44]S. Sun, "Mimo radar technology," in *Modern Radar for Automotive Applications*, edited by Z. Peng, C. Li, and F. Uysal (Institution of Engineering and Technology, 2022), Chap. 3, doi: 10.1049/sbra553e_ch3.

[45]The transceivers illuminate the environment and excite the backscatter tags, causing them to act as secondary transmitters. For ease of interpretation, however, it is helpful to view the transceivers as receivers and the backscatter tags as transmitters.

[46]W. J. Richardson, C. R. Greene Jr, C. I. Malme, and D. H. Thomson, *Marine mammals and noise* (Academic press, 2013).